M 2022

U.PORTO
FEUP FACULDADE DE ENGENHARIA
UNIVERSIDADE DO PORTO

OPTIMIZATION OF A HYDROGEN DRYING UNIT BY ADSORPTION PROCESSES

ANA LÚCIA LOUREIRO PINTO
MASTER THESIS IN CHEMICAL ENGINEERING
PRESENTED TO THE FACULTY OF ENGINEERING
OF THE UNIVERSITY OF PORTO

Master in Chemical Engineering

Optimization of a hydrogen drying unit by adsorption processes

Master dissertation

of

Ana Lúcia Loureiro Pinto

Developed within the course of dissertation

held in

Amnis Pura, Ltd

Supervisor at FEUP: **Prof. Adélio Mendes**

Joint supervisor at FEUP: **Dr. Paulo Ribeirinha**

Coordinator at Amnis Pura: **Dr. Frederico Relvas**

U.PORTO
FEUP FACULDADE DE ENGENHARIA
UNIVERSIDADE DO PORTO

DEPARTAMENTO DE
ENGENHARIA QUÍMICA

July 2022

Acknowledgment

First, I would like to thank Dr. Frederico Relvas and Dr. Paulo Ribeirinha for giving me the opportunity to learn so much and for all the support they gave me during the development of this dissertation. I would also like to thank Prof. Adélio Mendes for always challenging me and for the great support he always gave me.

To Tiago Santos for teaching me how everything worked in the lab and for always being available to help me. To the people working in labs E202, E101A and E101C, thank you for always giving me a hand and for the sense of cooperation I always felt. To José Pedro and Carlos, working in Amnis Pura, thank you for the constant concern and for the good working environment.

A special and most important thanks to my parents who have always given me the foundations I needed to reach all my goals. Thank you, mom, for never letting me give up, for the sense of resilience, and mainly for all the love. Thank you, dad, for your constant concern and for the stubbornness that I proudly inherited from you.

To my brother and my sister-in-law. Thank you Beto for being my forever safe haven, and for being the person I know I can count on unconditionally. Thank you Cláudia for the support you have always given me since I was a little girl and for all the conversations that have calmed me down and given me encouragement.

To my godparents for always giving me a second home and to my cousin Inês for being my personal cheerleader and for always taking care of me. To all my family who were always by my side, thanks to all of you who made me who I am today.

Finally, a special thanks to all my friends, the ones that always accompanied me and the ones I made during these 5 years at FEUP. I am eternally grateful for all the memories we created.

This work was financially supported by the Project "Baterias 2030" with the reference POCI-01-0247-FEDER-046846, co-financed by the Competitiveness and Internationalisation Operational Programme (COMPETE 2020), within the Partnership Agreement - Portugal 2020, through the European Regional Development Fund (ERDF).

Professor Adélio Mendes, supervisor of this dissertation, is an integrated member of LEPABE – Laboratory for Process Engineering, Environment, Biotechnology and Energy, financially supported by: LA/P/0045/2020 (ALiCE), UIDB/00511/2020 and UIDP/00511/2020 (LEPABE), funded by national funds through FCT/MCTES (PIDDAC).

Abstract

Reaching net-zero carbon emissions by 2050 implies an exponential growth in green technologies such as electrolysers and fuel cells. An electrolyser allows the splitting of water into oxygen and hydrogen. Hydrogen can then be used for energy storage, being further released through the reverse reaction to form water, in a fuel cell or gas turbine. The hydrogen that exits the electrolyser is, however, saturated with water that prevents its safe storage. So, it is necessary to include a drying step after the electrolysis, typically by Pressure Swing Adsorption (PSA), a well-established gas separation technology. Vacuum Pressure Swing Adsorption (VPSA) is a variant of PSA where the regeneration of the beds is performed under vacuum, which can be also used.

The main goal of this work is to optimize a laboratory PSA setup for hydrogen drying, optimising recovery and meeting the required purity of less than 5.00 ppm of water at the outlet hydrogen stream. Preliminary PSA and VPSA tests were performed in a two and three-column system packed with activated alumina, at 9 bar and a feed flow rate of 1.70 $L_N \cdot min^{-1}$ to evaluate the best configuration. The VPSA configuration with three columns was chosen for optimization by means of a Design of Experiences (DoE). The Response Surface Methodology was used to design 16 experiences – three factors and two levels – where the selected factors were the feed flow rate (1.50-2.00 $L_N \cdot min^{-1}$), purge to feed ratio (0-0.10) and adsorption time (100-180 s). The results were analysed using JMP software (SAS), which produced a second order polynomial fitting model and the statistical analysis. The VPSA optimum operating conditions were: feed flow rate of 1.50 $L_N \cdot min^{-1}$, a purge to feed ratio of 0.03 and an adsorption time of 142 s. These conditions resulted in a water content at the outlet of 4.00 ppm with a recovery of 85.6 %.

Additionally, a two-layer adsorbent configuration was also assessed. The bottom layer was loaded with activated alumina and the top layer with zeolite 13X. This test was performed under the same operating conditions of the test that achieved the highest recovery, performed only with alumina. A higher water content in the produced hydrogen was, however, obtained and no further experiments were performed.

The stoichiometric time (1461 minutes) and the breakthrough time (1050 minutes) were obtained, based on breakthrough experiments, allowing the determination of the efficiency and of the length of the mass transfer zone. The chosen operating conditions were the same as for the VPSA optimum conditions; the obtained adsorption separation efficiency and the length of the mass transfer zone were 55.1 % and 4.46 cm, respectively. It was concluded that the VPSA recovery can be improved using longer columns than the chosen ones.

Keywords: Hydrogen, PSA, VPSA, Purification, Optimization

Resumo

Atingir zero emissões de carbono até 2050 implica um crescimento exponencial de tecnologias não poluentes, tais como eletrolisadores e células de combustível. Um eletrolisador permite a decomposição da água em oxigénio e hidrogénio. O hidrogénio pode então ser utilizado para armazenamento de energia, sendo esta posteriormente libertada através da reação inversa para formar água, numa célula de combustível ou numa turbina de gás. O hidrogénio que sai do eletrolisador está, contudo, saturado com água, o que impede o seu armazenamento seguro. Assim, é necessário incluir uma etapa de secagem após a eletrólise, tipicamente por PSA, uma tecnologia bem desenvolvida de separação gasosa. VPSA é uma variante de PSA que também pode ser utilizada, em que a regeneração dos leitos é realizada sob vácuo.

O principal objetivo deste trabalho é otimizar uma instalação laboratorial de PSA para secagem de hidrogénio, otimizando a recuperação e atingindo a pureza requerida de menos de 5,00 ppm de água na corrente de saída de hidrogénio. Foram realizados testes preliminares de PSA e VPSA num sistema de duas e três colunas com alumina ativada, a 9 bar e com um caudal de alimentação de 1,70 $L_N \cdot min^{-1}$ para avaliar a melhor configuração. A configuração de VPSA com três colunas foi escolhida para otimização através de um DoE. A Metodologia de Superfície de Resposta foi utilizada para obter 16 experiências - três fatores e dois níveis - onde os fatores selecionados foram o caudal de alimentação (1,50-2,00 $L_N \cdot min^{-1}$), a razão purga/alimentação (0-0,10) e o tempo de adsorção (100-180 s). Os resultados foram analisados utilizando o *software* JMP (SAS), que produziu um modelo de ajuste polinomial de segunda ordem e a análise estatística. As condições ótimas de funcionamento do VPSA foram: caudal de alimentação de 1,50 $L_N \cdot min^{-1}$, razão purga/alimentação de 0,03 e tempo de adsorção de 142 s. Estas condições resultaram num teor de água à saída de 4,00 ppm com uma recuperação de 85,6 %.

Além disso, foi também avaliada uma configuração com duas camadas de adsorventes. A camada inferior com alumina ativada e a camada superior com zeólito 13X. Este teste foi realizado nas mesmas condições operacionais do teste que obteve a maior recuperação, realizado apenas com alumina. Foi, contudo, obtido um teor de água mais elevado produzido e não foram realizadas mais experiências.

O tempo estequiométrico (1461 minutos) e o tempo de rutura (1050 minutos) foram obtidos, com base em experiências de curvas de rutura, permitindo a determinação da eficiência e do comprimento da zona de transferência de massa. As condições de operação escolhidas foram as condições ótimas do VPSA; os valores obtidos para a eficiência de separação e para o comprimento da zona de transferência de massa foram de 55,1 % e 4,46 cm, respetivamente. Concluiu-se que a recuperação do VPSA pode ser melhorada utilizando colunas mais longas.

Palavras-Chave: Hidrogénio, PSA, VPSA, Purificação, Otimização

Declaration

I hereby declare, under word of honour, that this work is original and that all non-original contributions are indicated, and due reference is given to the author and source.

Porto, 31 July 2022

Ana Lúcia Loureiro Pinto

(Ana Lúcia Loureiro Pinto)

Index

List of Figures

List of Tables

Notation and Glossary

C	water concentration at the outlet	
C_0	water concentration at the inlet	
L_b	length of the adsorbent bed	cm
L_{MTZ}	length of the mass transfer zone	cm
L_{UB}	length of unused bed	cm
m_{ads}	mass of adsorbent	kg
n_r	number of response variables	
P	equilibrium pressure	bar
P_0	initial pressure	bar
P/F	purge to feed ratio	
q	adsorption capacity	$mol \cdot kg^{-1}$
Q	flow rate	$m^3 \cdot s^{-1}$
q_{bp}	column capacity until breakpoint	$mol \cdot kg^{-1}$
Q_{feed}	feed flow rate	$L_N \cdot min^{-1}$
$Q_{product}$	product flow rate	$L_N \cdot min^{-1}$
Q_{purge}	purge flow rate	$L_N \cdot min^{-1}$
q_{tot}	column total capacity	
R^2	determination coefficient	
R_H	relative humidity	%
R_{rec}	product recovery	%
t	time	
t_1	step time	s
t_{ads}	adsorption time	s
t_{bp}	breakthrough time	min
t_{pg}	purge time	s
t_{st}	stoichiometric time	min
X	coded variable	
y	water concentration	ppm
y_0	water concentration at the inlet	ppm
y_n	response of an output variable	

Greek Letters

β	regression coefficient
β_0	offset term
η	column efficiency

Indexes

n	number of output variable
i	number of parameter
j	number of parameter

List of Acronyms

AD	Adsorption
AEM	Anion Exchange Membrane
ANOVA	Analysis of Variance
BD	Blowdown
BF	Backfill
CCUS	Carbon Capture, Utilization and Storage
DoE	Design of Experiences
DPE	Pressure Equalization

EU	European Union
IEA	International Energy Agency
MFC	Mass Flow Controller
MFM	Mass Flow Meter
MTZ	Mass Transfer Zone
NREL	National Renewable Energy Laboratory
NZE	Net-Zero Emissions
PC	Pressure Controller
PEM	Polymer Electrolyte Membrane
PG	Purge
PGV	Vacuum Purge
PPE	Pressure Equalization
PSA	Pressure Swing Adsorption
PT	Pressure Transducer
SAS	Statistical Analysis System
TC	Temperature Controller
TFC	Total Final Energy Consumption
TSA	Temperature Swing Adsorption
TT	Temperature Transducer
VPSA	Vacuum Pressure Swing Adsorption

1 Introduction

1.1 Framing and presentation of the work

It is widely accepted by the scientific community that the future of the energy sector cannot depend entirely on non-renewable sources. Firstly, because this type of energy, as the name implies, is consumed at a faster rate than it is produced. In addition, non-renewable energy sources, such as fossil fuels, are associated with the emission of polluting gases into the atmosphere, causing irreversible damage. Therefore, a change in the energy paradigm is imperative in order to gradually increase the share of renewable energy[1].

Hydrogen is an energy vector that has the potential to contribute to this change through its use in the transport, industry and energy sectors[2]. The way hydrogen is produced, however, also has a major impact regarding the emission of pollutants into the atmosphere. Depending on the production process, hydrogen can be categorized into colours as illustrated in Figure 1.1[3].

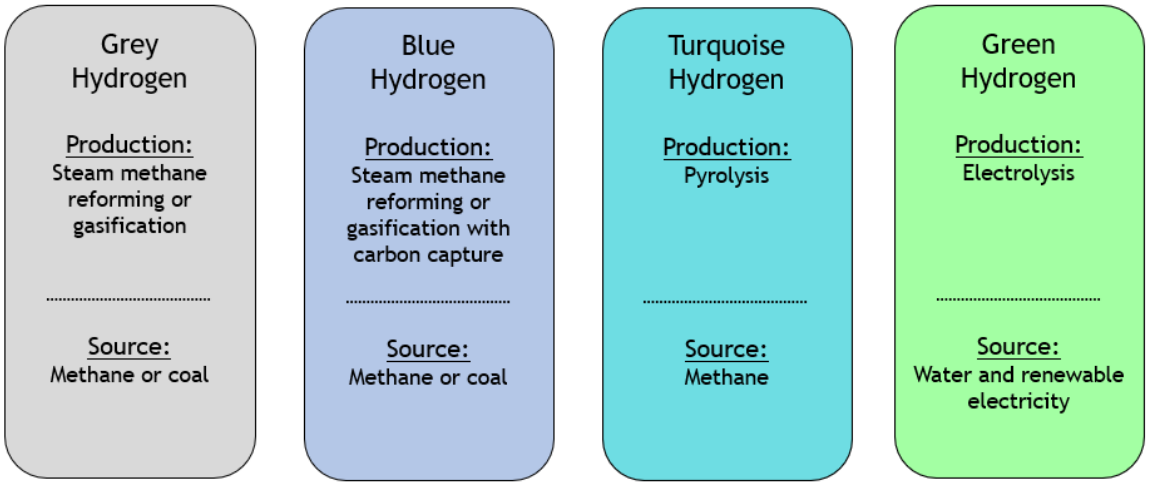

Figure 1.1. Hydrogen colours system. Adapted from (International Renewable Energy Agency, 2020)[3]

Among the various colours, hydrogen produced using electricity from renewable sources is called green hydrogen. The schematic in Figure 1.2 illustrates the integration of green hydrogen into a zero-carbon energy system. Electricity is used to electrolyze water leading to the formation of oxygen and hydrogen. Considering that electricity is produced from renewables, e.g. solar or wind energy, the process can be considered as carbon-neutral[4].

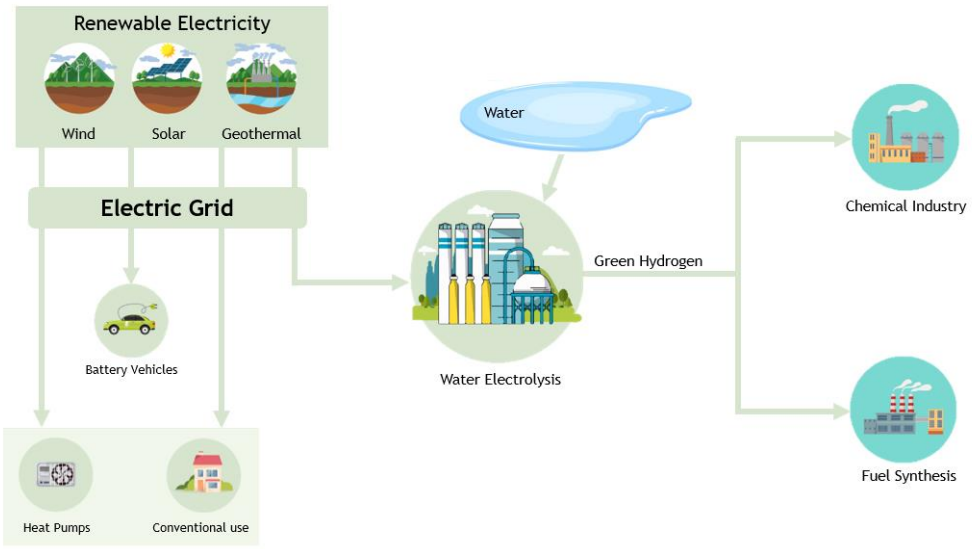

Figure 1.2. Integration of green hydrogen into a zero-carbon energy system. Adapted from (CIC EnergiGUNE, 2022)[5].

Electrolysis is, however, still a field under investigation and in continuous evolution. The hydrogen coming from the electrolyser still has impurities and cannot be stored immediately. Nitrogen, oxygen and water vapor are the three main contaminants in the electrolyser output stream, the last one being one of the most difficult component to remove[6]. It is in this context that Pressure Swing Adsorption (PSA) technology appears, allowing for hydrogen drying through cyclic pressure changes in a packed column with a certain adsorbent.

Accordingly, the main purpose of this work is the optimization of a PSA installation in order to obtain a hydrogen stream that meets the legal requirements of ISO 14687:2019, that is, obtaining a hydrogen stream with less than 5 ppm of water[7]. More specifically, the main objectives/tasks of this study were:

- Preliminary PSA tests to identify the best PSA configuration.
- Optimization of the process using a design of experiences.

This work follows a previous thesis where a hydrogen drying system by PSA was developed. Different adsorbents were selected and characterized to choose the one that had the best behaviour regarding hydrogen drying. Alumina was selected as the best adsorbent due to its higher steady state capacity. Some PSA tests were also performed with two columns which did not allow reaching the purity goal in the outlet stream.

1.2 Presentation of the company

Amnis Pura is a spinoff company from the Faculty of Engineering of University of Porto and is one of the first companies dedicated to the development and commercialization of hydrogen

technologies. The company is settled on 25 years of experience in PSA technology and more than 15 years in fuel cells applications.

With a strong R&D mindset, Amnis Pura foresees to be a brand of reference in the international market of hydrogen purification and sustainable energy, pushing the hydrogen economy to the future.

1.3 Contribution of the author to the work

I adapted the experimental PSA setup that was only suitable to non-condensing gases in order to work with water vapor. I also modified the initial arrangement of the top valves which did not allow for purge and backfill steps to occur at the same time. The current layout allows all the steps to be done between all the columns simultaneously.

I performed all the PSA and VPSA tests mentioned in this dissertation and did all the data and statistical analysis.

1.4 Organization of the dissertation

This dissertation is outlined as follow:

- In chapter one, *Introduction*, a brief framework is given for the dissertation subject and the working goals of the dissertation are presented.
- In chapter two, *Context and State of the art*, a background on the dissertation theme is presented by means of a review of the most relevant literature concerning the importance of hydrogen, electrolysis as a way to obtain green hydrogen and PSA technology as well as its variants.
- In chapter three, *Materials and Methods*, the installation used to carry out the tests is presented in detail and the methodology used to achieve the proposed objectives is explained, that is, the cycles and conditions used in each test are described, as well as the conditions under which the adsorbent was regenerated so that it could be used.
- In chapter four, *Results and Discussion*, the results of the preliminary tests are outlined and discussed as well as the results of the tests performed to optimize the installation.
- In chapter five, *Conclusions*, the main resolutions attained in this work are presented.
- At last, in chapter six, *Assessment of the work done*, an evaluation of the work that was developed is done. The accomplished goals are outlined and suggestions for future work are given.

2 Context and State of the art

Global warming, caused by the increasing emissions of polluting gases, has led most of the world's population to worry about how the energy consumed is produced and the consequences that result from this production. In this way, several countries are currently investing in the implementation of clean and renewable energies to decarbonize their energy system and mitigate the effects of global warming[8,9].

The Paris Agreement establishes a framework to prevent dangerous climate change, by restricting the global temperature rise to far less than 2 °C and pushing ahead with further efforts to limit it to 1.5 °C, compared to pre-industrial levels. To achieve this goal, the countries that are part of this agreement must reduce greenhouse gas emissions into the atmosphere to "net-zero" (NZE), by 2050[10]. This scenario implies adopting an energy policy based on the following pillars[11]:

- Energy efficiency
- Behaviour change
- Electrification
- Renewable energies
- Hydrogen and hydrogen-based fuels
- Carbon capture, utilization and storage (CCUS)

According to the International Energy Agency (IEA) Global Hydrogen Review, hydrogen will play a key role in driving the NZE scenario through the increase in its contribution to the total final energy consumption (TFC). By 2050, hydrogen and hydrogen-derived fuels are expected to contribute 10 % to TFC, up from the 0.1 % observed in 2020. It is necessary, however, that this rise is accompanied by an evolution in the production processes of hydrogen so that it may indeed become a green energy vector[11].

2.1 Hydrogen production

Most of today's hydrogen is produced from fossil fuels or from by-products of the petrochemical industry. According to the IEA, of the 90 Mt of hydrogen produced in 2020, 80 % was from fossil fuels and the rest was almost entirely derived from gases generated in the refinery and petrochemical industries. That is equivalent to the emission of almost 900 Mt of CO_2[11].

Even though low-carbon hydrogen production is currently an insignificant part of the total hydrogen production, there are several technologies linked to this type of production, namely[11]:

- Water electrolysis.
- Through fossil fuels with CCUS.

- Through biomass gasification.

By 2050, hydrogen production is expected to be mostly met by the above mentioned technologies and reach 500 Mt[11]. Figure 2.1 shows the share of each hydrogen source in 2020 and the forecast evolution by 2050.

Nowadays, water electrolysis is seen as the most promising process for producing high-purity green hydrogen. In the near future, electrolysis is expected to be the main hydrogen production process for decentralized applications, such as hydrogen fuelling stations[11,12].

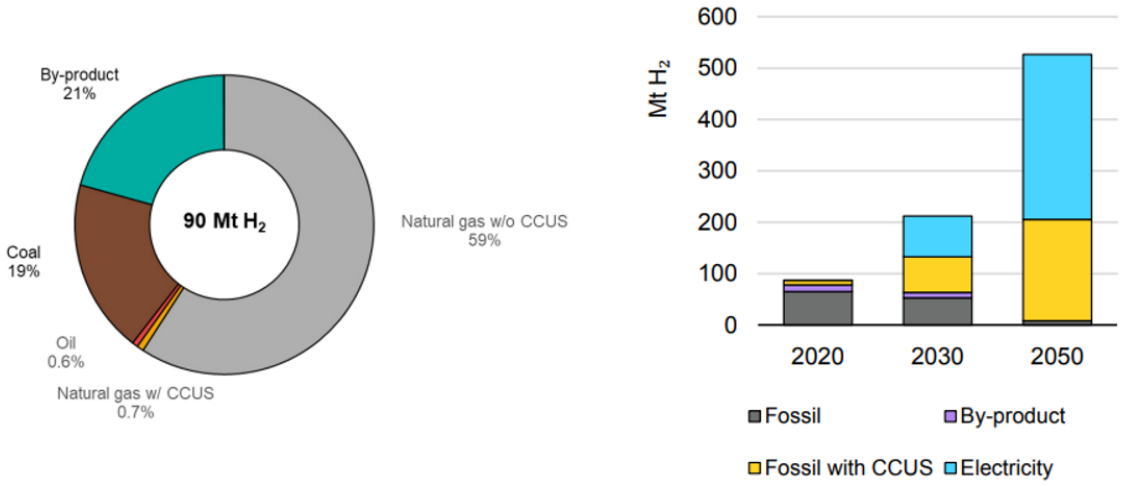

Figure 2.1. Sources of hydrogen production in 2020 (at the left) and in the NZE scenario, 2020-2050 (at the right). Extracted from (International Energy Agency, 2021)[11].

According to the IEA report, NET Zero by 2050 – A Roadmap for the Global Energy Sector, achieving the goal of NZE by 2050 will require the production of ca. 306 Mt of green hydrogen each year. To make this possible, technology related to the production of hydrogen by water electrolysis needs to improve[13,14]. The European Union (EU) sets out a roadmap that seeks to meet this challenge through several phases:

- During a first phase, from 2020 to 2024, the goals consist in installing at least 6 GW of green hydrogen electrolysers and producing up to 1 Mt of green hydrogen. The purpose of this phase is the decarbonisation of the existing hydrogen production[15].
- In the second phase, from 2025 to 2030, EU aims to install at least 40 GW of green hydrogen electrolysers and to produce up to 10 Mt of renewable hydrogen. At this point, renewable hydrogen would become cost-competitive with other production processes[15].
- In a third phase, from 2030 to 2050, the renewable hydrogen production processes would reach maturity and would be widely implemented to cover all hard-to-decarbonise sectors[15].

2.2 Hydrogen from water electrolysis

As it was already mentioned, water electrolysis is seen as a promising method to produce hydrogen whose working principle is based on the decomposition of water into ions according to Equation 2.1[8]. This reaction is, however, very endothermic and it is necessary to provide electrical current, which, being supplied by renewable energy sources, makes this method the most promising for a sustainable hydrogen production[8,16].

$$2H_2O\,(\text{liquid}) \rightarrow 2H_2(\text{gas}) + O_2(\text{gas}) \qquad (2.1)$$

As this is an endothermic reaction, energy can be absorbed and stored in the form of chemical hydrogen bonds. The reverse reaction, forming water, is on the other hand exothermic, and releases energy. In this way, it is possible to store renewable energy with hydrogen[17].

Electrolysis of water occurs in an electrolyser, which consists of a cathode and an anode (electrodes) immersed in an electrolyte and separated by a porous membrane. When electric current is applied to the electrodes, the water splits and hydrogen is produced at the cathode and oxygen at the anode[16,18]. There are essentially three different electrolysis methods for producing hydrogen through water electrolysis[19]:

- Alkaline Electrolysis

Alkaline electrolysis is a well-established technology in hydrogen production at MW scale, representing the most globally used commercial electrolysis technology. It uses an alkaline electrolyte (typically KOH) and a diaphragm permeable to hydroxide ions and water, allowing the separation of produced gases. However, the diaphragm does enable some crossover from one half-cell to the other which can be particularly problematic at low loads. Lowering the oxygen production increases the hydrogen crossover concentration which can reach dangerous levels, since the lower explosion limit of hydrogen is 4 mol %[9,20].

- Polymer Electrolyte Membrane (PEM) Electrolysis

PEM electrolysis is a technology already available on the market and growing fast. It uses a solid polymer electrolyte and it is more flexible than alkaline electrolysis, being able to operate in a wider range and having less response time. This flexibility offers a potentially new multi-market electricity income stream to compensate for the higher outlay cost compared to alkaline electrolyzers[9]. Therefore, PEM electrolysis offers a good solution for sustainable hydrogen production, and is suitable to work with renewable energy sources such as wind and solar[21]. A PEM electrolyser is schematically shown in Figure 2.2.

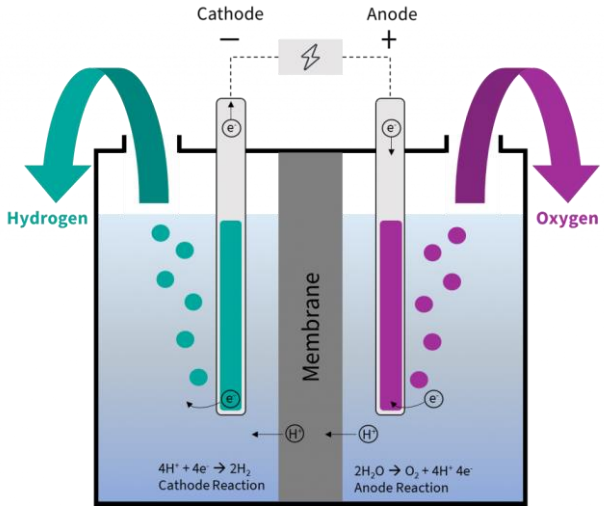

Figure 2.2. Schematic of a PEM electrolyser. Extracted from (Hussy, 2022)[22].

- Solid Oxide Electrolysis

Solid oxide electrolysis uses a proton-conducting ceramic membrane to separate the two half-cells. It is a more energy-efficient mechanism when compared with alkaline and PEM electrolysis but it is still in an early stage of development[9].

Table 2.1 shows the half-reactions that occur at the electrodes depending on the type of electrolysis and the temperature range at which they operate.

Table 2.1. Half-reactions and typical temperature ranges of different types of water electrolysis[9,23].

Type of Electrolysis	Temperature (K)	Half-reactions	
		Cathode	Anode
Alkaline	333-363	$H_2O + 2e^- \rightarrow H_2 + 2OH^-$	$2OH^- \rightarrow \frac{1}{2}O_2 + H_2O + 2e^-$
PEM	293-373	$2H^+ + 2e^- \rightarrow H_2$	$H_2O \rightarrow \frac{1}{2}O_2 + 2H^+ + 2e^-$
Solid Oxide	973-1273	$H_2O + 2e^- \rightarrow H_2 + O^{2-}$	$O^{2-} \rightarrow \frac{1}{2}O_2 + 2e^-$

In addition to these three main technologies, there is currently a new type of electrolysis being studied that aims to challenge PEM electrolysis as state-of-the-art in water electrolysis. It uses an anion exchange membrane (AEM) and operates at temperatures below 100 ºC. Although combining the advantages of alkaline and PEM electrolysis: it has a membrane that separates the electrolytes (PEM) and uses non-noble metals as electrocatalysts (alkaline), AEM is still at a very early stage of development and improvements are still needed. The AEM electrolysis process is schematised in Figure 2.3 together with a comparison with the PEM process[20,24,25].

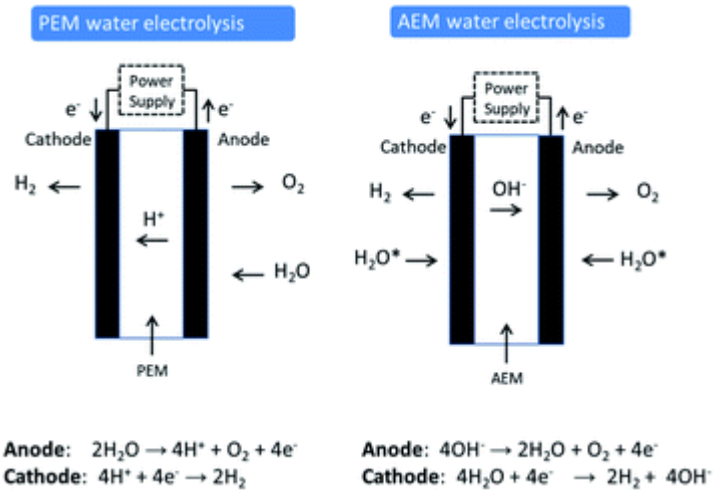

*Figure 2.3. Comparison between PEM and AEM electrolysis. *Water feed of AEM is usually combined with an electrolyte (HCO^{3-}/CO_3^{2-} or dilute KOH) to obtain sufficient performance. Extracted from (Miller, et al., 2020)[20].*

2.3 Hydrogen purification

Hydrogen produced by water electrolysis is typically contaminated with nitrogen, oxygen, and water. Typical content of each one of these contaminants and content allowed for storage are shown in Table 2.2 as well as their origin and treatment process. Among these treatment processes, the one of water removal (hydrogen drying) is one of the least studied and reported in the literature and, yet one of the most important ones. That is because hydrogen should contain an amount of water that does not allow for condensation when stored at high pressures, as stated in ISO 14687:2019[6,7,26,27]. In the case of automotive grade hydrogen, where hydrogen is stored at 350 bar or 700 bar, the standard sets the water content as a maximum of 5 ppm, thereby corresponding to a dew point of -66 °C[7].

Different technologies can be used for gas drying, namely membrane processes, gas cooling and adsorption-based processes. In this regard, gas cooling is not the best option to achieve the desired goal for water removal since water forms ice at low temperatures. Membrane processes are expensive and not very flexible. Besides, they do not achieve the desired level of purity[6]. Adsorption processes such as TSA or PSA are typically the best options, since hydrogen is a weak adsorbate and does not significantly affect the adsorption of water[6,26]. The difference between the two processes is essentially the mechanism that allows the adsorption to take place. In TSA, since the adsorption process is exothermic, a decrease in temperature, favours the adsorption of water and, while an increase in temperature favours the regeneration of the adsorbent. In PSA, on the other hand, the adsorption is achieved by increasing the pressure and the regeneration by lowering it. Overall, PSA offers advantages over TSA since the latter has slower cycles due to the time required to allow for temperature changes while also requiring a high energy consumption to increase the temperature of the system[27].

Table 2.2. Typical contaminants of hydrogen produced from water electrolysis: allowed content for storage, typical content, origin and treatment process[6,26].

Contaminant	ISO 14687:2019 threshold	Typical content	Origin	Treatment Process
Nitrogen	300 ppm	<100 ppm after initial purge	Purge and inertization Feed Water	Venting initial production
Oxygen	5 ppm	2000-6000 ppm	Gas solubility Crossover	Catalytic Recombination $O_2 + 2H_{2\,cat} \rightarrow H_2O$
Water	5 ppm	>2000 ppm, saturated at ambient temperature	Process	Gas cooling Membrane processes PSA or TSA(1)

(1)TSA – Temperature Swing Adsorption

2.3.1 Hydrogen drying by pressure swing adsorption (PSA)

A basic PSA process follows the Skarstrom cycle, which consists of four elementary steps (pressurization, production, depressurization, and purging) in which two columns operate together and 180° apart[28]. A scheme of a typical Skarstrom PSA is represented in Figure 2.4. The 4 steps of the Skarstrom cycle are described below and schematize in Figure 2.5.

- Pressurization

With the top valve closed, the mixture is fed to the column, increasing the column pressure. The component with higher adsorption affinity (heavy component - water) is removed from the gas phase and the component that is worst adsorbed (light component - hydrogen) is concentrated near the top of the column. When the desired operating pressure is reached, this step ends[28].

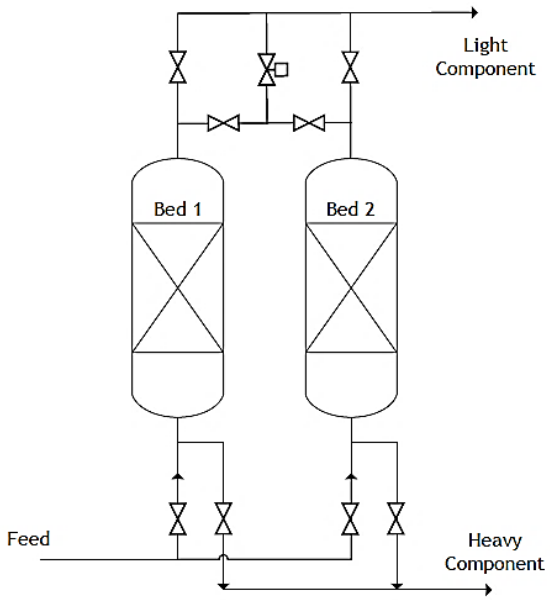

Figure 2.4. Skarstrom PSA cycle.

- Production

The valve at the top of the column is opened and a gaseous stream rich in the light component comes out, while the heavy component is adsorbed. This step ends just before the heavy component reaches the top of the column (breakthrough)[28].

- Depressurization

The top valve is closed again and the gas enriched in the heavy component exits through the bottom, causing the column pressure to decrease[28].

- Purge

A stream rich in the light component is passed through the top of the column and causes the partial pressure of the heavy component to drop, allowing it to desorb. Because of the mismatch between the two columns, some of the current rich in the light component that is being produced in the adjacent column is used at this stage[28].

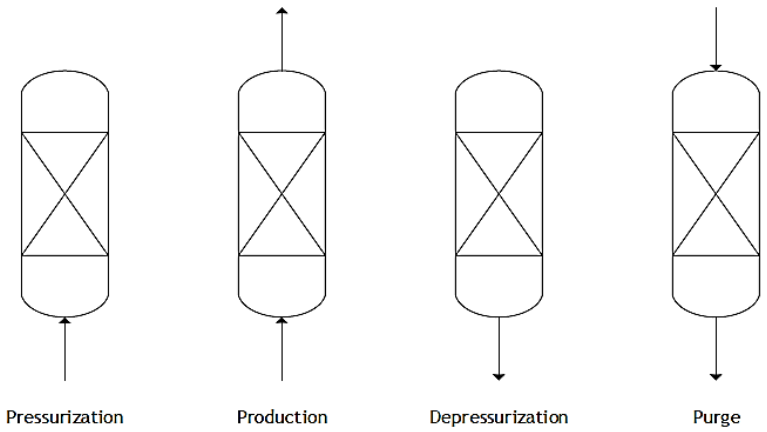

Figure 2.5. Elementary steps of a Skarstrom PSA cycle.

The Skarstrom cycle can be modified by introducing an equalization step. This step is introduced after the production step and the purge step. After the production step, the column still has a quantity of gas at the top that has no product quality but is still quite rich in the light component. So, instead of directly depressurizing this first column, this one is connected to a second column, which has finished the purge step, and the pressure is equalized. This way, the first column partially pressurizes the second column, decreasing the energy consumption that is required to pressurize it and reducing the losses from the depressurization step, consequently increasing the recovery of the light component[26,28]. The sequence of operation steps with pressure equalization is represented in Figure 2.6. Using this step in a process with only two columns does not allow for continuous production and is therefore commonly implemented only in processes with three or more columns[29].

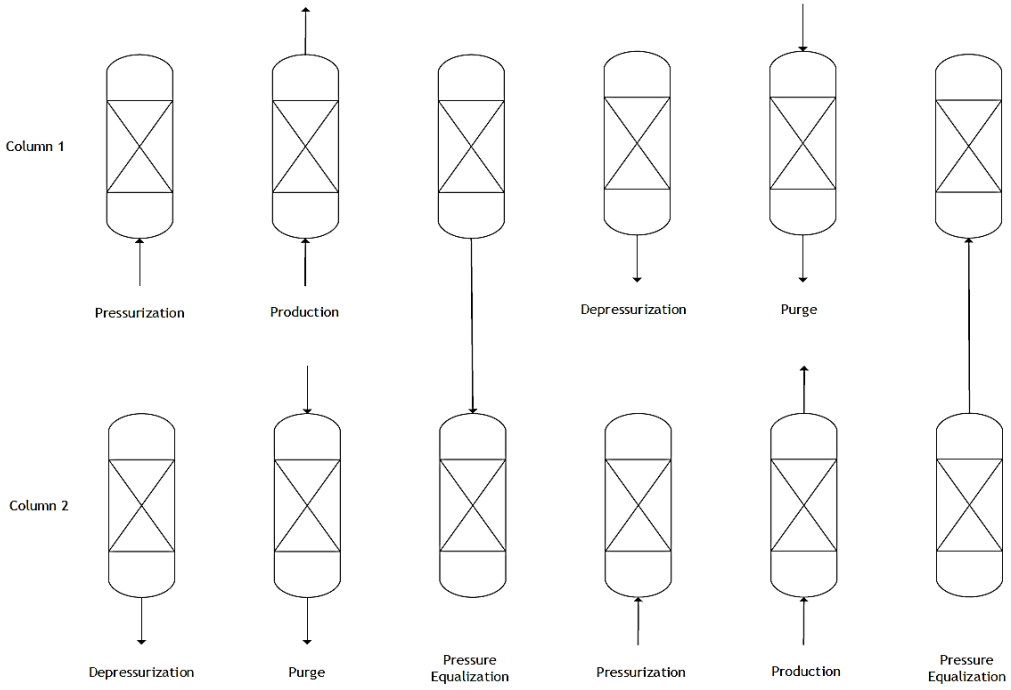

Figure 2.6. Operation steps of a Skarstrom PSA cycle with pressure equalization.

Besides the equalization step, a backfill step is usually considered too. In this stage, schematically represented in Figure 2.7, the column that finished the adsorbent regeneration step is pressurized with part of the product stream from a first column, in counterflow. Unlike pressure equalization, backfill allows production to take place in one column while the other one is pressurized, permitting continuous production even in processes with only two columns[29].

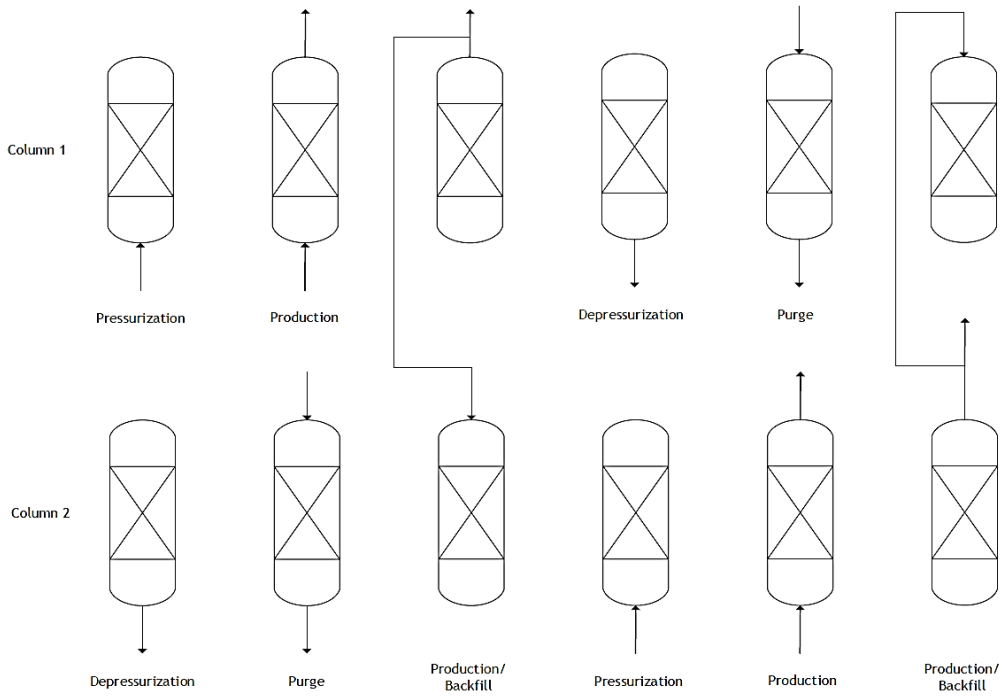

Figure 2.7. Operation steps of a Skarstrom PSA cycle with a backfill step.

In order to increase the column regeneration, and therefore the process efficiency, it is also possible to add an evacuation step after the depressurization, replacing (or complementing) the purge stage. To do this, a vacuum pump is installed at the off-gas stream. This process is a variant of the PSA process called Vacuum Pressure Swing Adsorption (VPSA). At the same high pressure and for the same desired product purity level, losses of the light component are lower in VPSA when compared to the losses in the purge step of a basic Skarstrom cycle. Consequently, there is a higher recovery of the component that is less adsorbed at the expense of a higher energy cost required for the operation of the vacuum pump[26].

Regarding hydrogen drying, in commercially available electrolysis systems, a fixed orifice is used in the purge step that allows for the amount of hydrogen passing from one column to the other to be constant, regardless of the hydrogen production in the electrolyser. However, if the electrical energy required for electrolysis is supplied by renewable sources, the electrolyser will operate most of the time below full capacity, but the amount of hydrogen passing through the orifice will be the same. Since this hydrogen will only be used for purging the column adjacent to the one that is producing, if the hydrogen production decreases but the amount passing through the orifice is the same, a higher fraction of hydrogen is lost at this stage[30]. With

this method, losses in the order of 3.5 % of the nominal hydrogen flow occur. The United States National Renewable Energy Laboratory (NREL) proposed an alternative approach to the calibrated orifice that consists of varying the hydrogen flow that will purge the adjacent column according to the amount of hydrogen being produced and that aims to keep the hydrogen purge losses at 3.5 % of the actual hydrogen flow instead of 3.5 % of the nominal flow. Comparative tests of the two techniques (fixed orifice and variable flow) showed that the NREL approach can save 2-10 % more hydrogen than the fixed orifice approach[31].

Recently, a hydrogen VPSA drying system was implemented and tested in a combined service station for battery electric & hydrogen fuel cell vehicles. Using molecular sieves 4A as adsorbent and operating at room temperature and 40 bar, this system allows to obtain hydrogen with less than 0.1 ppm of water and a 98.4 % recovery with an energy consumption of only 0.5 $kWh \cdot kg_{H2}^{-1}$ [6,32].

2.3.1.1 Adsorbents

There are several adsorbents that can be used for separations by cyclic adsorption processes. The adsorption phenomena can either result from chemical reaction (chemisorption) or through weak intermolecular van der Waals forces (physisorption). Among adsorbents, the most widely used are silica gel, activated alumina and zeolites. The main physical properties of these materials are summarized in Table 2.3. Regarding water adsorption, Table 2.3 shows that the adsorbent materials that allow obtaining a hydrogen current with a lower dew point also have higher heat of adsorption, i.e., a drying system that allows obtaining a lower dew point comes with the consequence of a higher energy consumption[33].

Table 2.3. Main physical properties of typical adsorbents used in water vapor adsorption[33-35].

Properties	Silica Gel	Activated Alumina	Zeolites
Bulk density ($kg \cdot m^{-3}$)	721	833-881	641-721
Average porosity (%)	50-65	0.24	0.2
Surface area ($m^2 \cdot g^{-1}$)	720-760	210	-
Particle shape	Granular	Granular	Cylindrical pellets
Dew point (ºC)	-60	-70	-100
Heat of adsorption ($kJ \cdot kg_{H2O}^{-1}$)	3256	3722	4187

The adsorption capacity (q) of a given material for a given compound at a certain concentration (P/P_0) is represented by its adsorption isotherm. Since chemisorption is an irreversible process, despite the cyclic regeneration to which the adsorbents are subjected, these will always be contaminated with a fraction of contaminant, causing their adsorption capacity to progressively

decrease along the cyclic process. After a few cycles they reach a steady state, the so-called cyclic steady state. Thus, the isotherms that should be considered when designing a PSA system should be effective isotherms, i.e., the adsorbent should have already experienced a cyclic adsorption process. The effective adsorption isotherms of water vapor on the aforementioned adsorbents are represented in Figure 2.8. Comparing the three types, (Ferreira, et al., 2011)[36] concluded that silica gel is the material with the lowest water contamination, followed by activated alumina and zeolites[36].

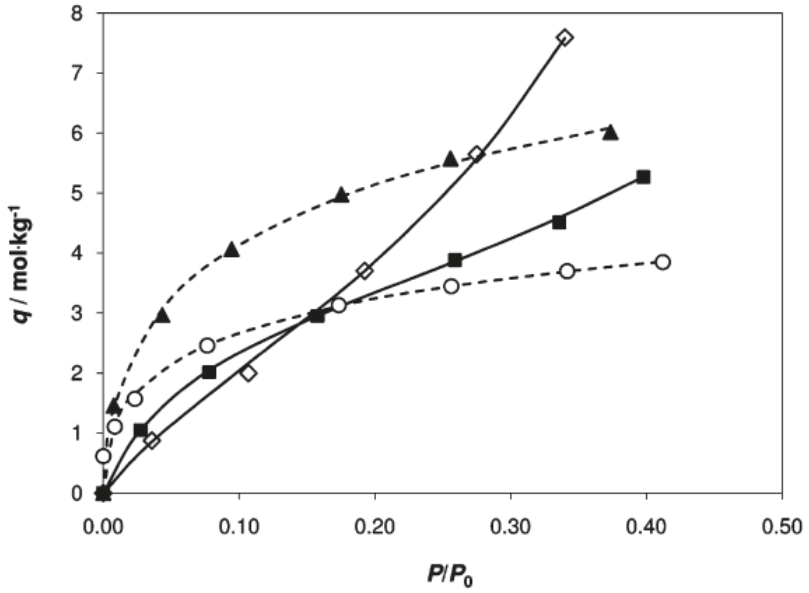

Figure 2.8. Water vapor effective isotherms at 35 ºC on zeolites (▲ and ○), silica (◊) and alumina (■). Extracted from (Ferreira, et al., 2011)[36].

The most used configuration of adsorbents in PSA systems for hydrogen drying consists of an initial layer of silica gel or activated alumina followed by a layer of zeolites. That is because zeolites have the advantage of having a high adsorption capacity even when the component to be adsorbed is in low concentrations. Corroborating this statement, (Rege, et al., 2001)[37] concluded that a configuration with a layer of activated alumina and another layer of zeolite 13X gave better results when compared to using a bed of one of these adsorbents alone[33,36,37].

In this work, all the main PSA and VPSA tests will be performed using activated alumina. An additional test will also be performed using a layer of activated alumina followed by a layer of zeolite 13X.

3 Materials and Methods

In this chapter, the materials and equipment used in the course of this work are presented. The methods used are also explained so that afterwards it is possible to understand and analyse the results obtained.

3.1 Adsorbents

The adsorbent used in all the preliminary and optimization tests was activated alumina SYLOBEAD® AA 102 supplied by W.R. Grace. Typical properties of this material are given in Table 3.1.

Table 3.1. Typical properties of activated alumina SYLOBEAD® AA 102. Extracted from (Grace, 2017)[38].

Property	Value
Bulk density ($g \cdot L^{-1}$)	770
Surface area ($m^2 \cdot g^{-1}$)	340
Porosity	0.4-0.5
Bead size (mm)	1.5-3

Before packing the columns, activated alumina was activated/regenerated under controlled temperature and dry atmosphere. For the purpose, a Termolab horizontal tubular furnace was used, and a sample of the material was heated in a nitrogen atmosphere at a flow rate of 400 $mL \cdot min^{-1}$. The heating rate used was 1 $ºC \cdot min^{-1}$ with a final temperature of 320 ºC and soaking time of 720 min[27].

For the additional VPSA test with two adsorbents, the materials used here were activated alumina SYLOBEAD® AA 102 and zeolite MERYT MS-13X, supplied by MERYT Catalysts & Innovation. Typical properties of a zeolite 13X are presented in Table 3.2.

Table 3.2. Typical properties of zeolite 13X. Extracted from (BASF, 2020)[39].

Property	Value
Bulk density ($g \cdot L^{-1}$)	655-700
Bead size (mm)	2.5-5

The zeolite was regenerated using the same method applied for the activated alumina, but with a final temperature of 375 ºC[27].

The water vapor isotherms of both adsorbents were obtained by (Bexiga, 2021)[27], at 50 ºC, and are represented in Figure 3.1 and 3.2, for activated alumina and zeolite 13X, respectively.

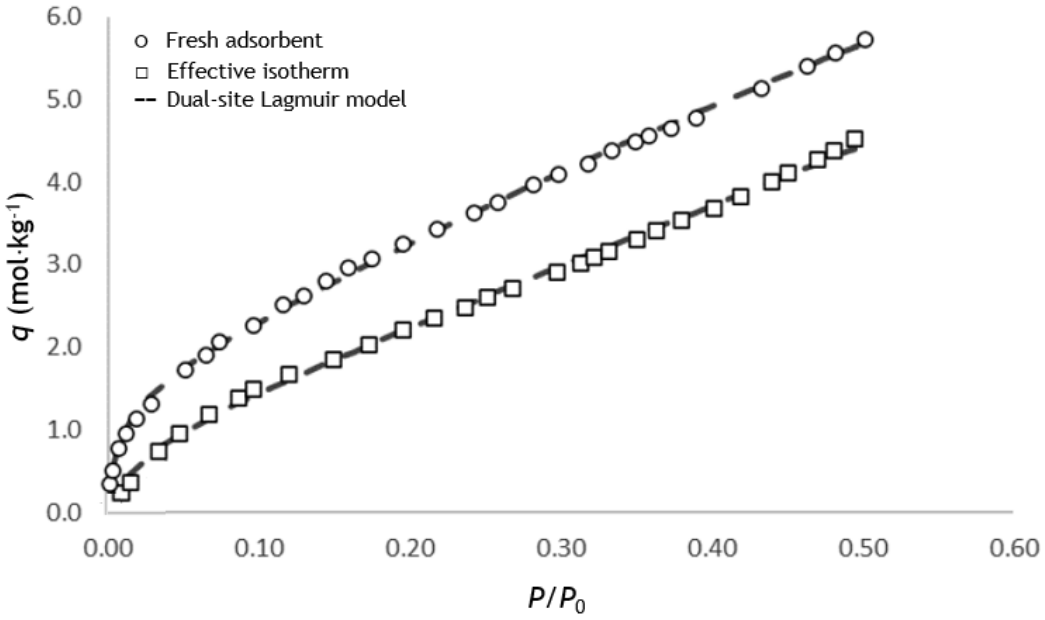

Figure 3.1. Water vapor adsorption isotherms at 50 ºC on activated alumina SYLOBEAD® AA 102. Adapted from (Bexiga, 2021)[27].

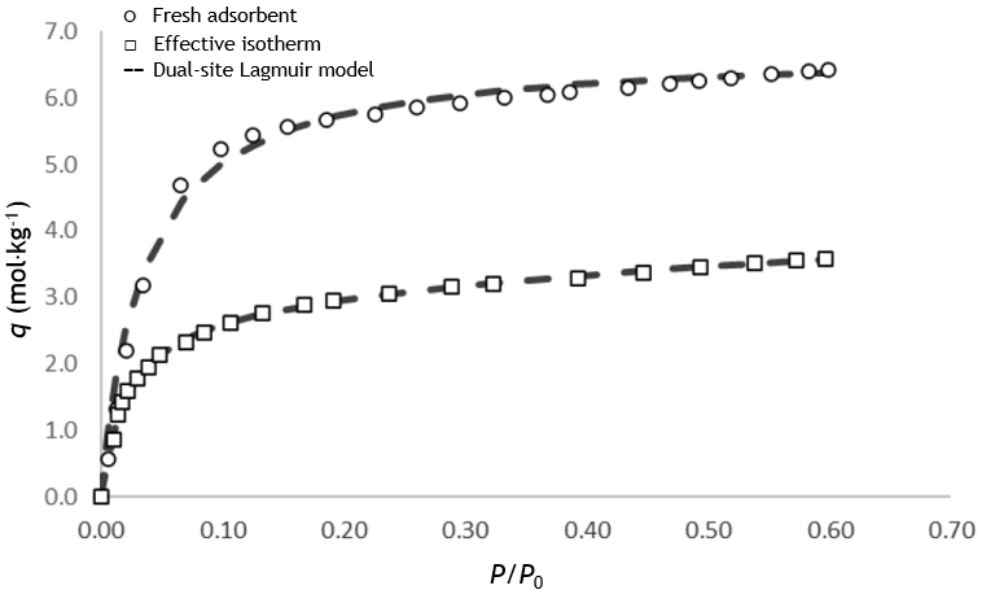

Figure 3.2. Water vapor isotherms at 50 ºC on zeolite 13X MERYT MS-13X. Adapted from (Bexiga, 2021)[27].

3.2 Setup used in the PSA and VPSA tests

The experimental setup used for the PSA and VPSA tests is shown in Figure 3.3. Although the setup was prepared for up to four-column, only two and three-column tests were performed.

All columns were made of steel and had the same dimensions, i.e., an internal diameter of 2.69 cm, a height of 7.95 cm and a wall thickness of 0.16 cm.

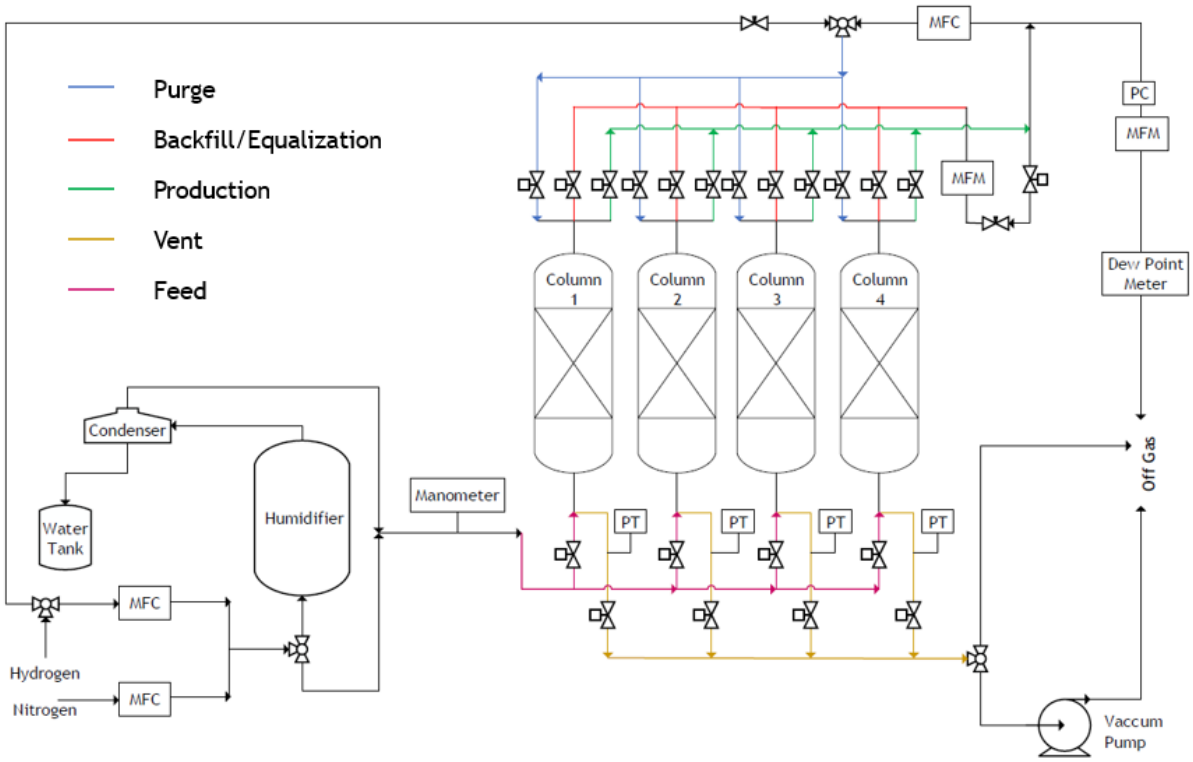

Figure 3.3. Process flow diagram of the setup used in all the PSA and VPSA tests.

The gases (nitrogen and hydrogen) were all supplied by Air Liquide. The hydrogen feed stream includes a manual three-way valve that allows routing to the feed mix stream or to the purge stream. The purge line also comprises a needle valve to control the flow of pure hydrogen that purges the columns. Both hydrogen and nitrogen feed flowrates are controlled through mass flow controllers (MFC). The feed stream then goes to a manual three-way valve that allows for it to be fed without humidification (by-passing the humidifier), or to go through the humidifier. The humidifier is in series with a condenser, followed by a water storage tank avoid condensation in the PSA feed stream.

The humidification capacity of the humidifier was read using a gas flow rate of 1.50 $L_N \cdot min^{-1}$, before the drying tests, using a hygrometer located at its outlet stream. The water height in the humidifier was 18 cm and the column diameter was 15 cm.

A manometer was placed at the feed stream for pressure monitoring. The feed stream (pink line) then enters the columns passing through a solenoid valve. All the columns are equipped with pressure transducers (PT) placed in the bottom side. The vent stream (yellow line), equipped with solenoid valves, allows the gases to exit the column from the bottom side and is

connected to a three-way electric valve which allows the gas to exit the column either at atmospheric pressure or under vacuum, by passing through a vacuum pump.

At the top, each column is connected to three lines: product, purge and backfill/equalization, all of them equipped with solenoid valves. When the gas leaves the product line (green line), it first passes through a pressure controller (PC), a mass flow meter (MFM) and through the dew-point meter. However, some of the product can be used to purge a column. In this case, the purge flow rate is controlled using a MFC. Furthermore, part of the product can also be used for backfilling. Here, the backfill gas (red line), passes through a solenoid valve and is further regulated using a needle valve. A MFM is placed afterwards for measuring the backfill flow rate. The backfill line is also used for equalisation. In this case, the solenoid valve connected to the product line is closed, and the corresponding valves of two columns under pressure equalization step are opened.

The off gas of the installation consists of an exhaust system that routes the gases safely to the outside.

The mass flow and pressure controllers as well as the mass flow and pressure meters are connected to a LabView routine on the computer that assists the installation. The LabView routine acquires the signals and controls the experimental setup, enabling a constant display of all the operating variables. All the solenoid valves are controlled by a VBA routine that is also installed in the auxiliar computer. The specifications of all the controllers and meters are detailed in Appendix A as well as of the vacuum pump and the dew point meter.

3.3 PSA and VPSA tests

For each PSA or VPSA test, data regarding relative humidity, water concentration and dew point were obtained from the dew point meter as a measure of product stream purity. Moreover, through the acquisition of data in LabView concerning the product and feed flow rate, recovery (R_{rec}) was also calculated using Equation 3.1, where $Q_{product}$ is the product flow rate and Q_{feed} is the feed flow rate.

$$R_{\mathrm{rec}} = \frac{\int Q_{\mathrm{product}}\,\mathrm{d}t}{\int Q_{\mathrm{feed}}\,\mathrm{d}t} \tag{3.1}$$

3.3.1 Preliminary Tests

All preliminary PSA and VPSA tests were performed using ca. 31.58 g of activated alumina in each column with a feed flow rate of 1.70 $L_N \cdot min^{-1}$ and at a high pressure of 9 bar. The remaining conditions for each test are outlined in Table 3.6.

Initially, using only two columns, two different cycles were tested, both illustrated in Table 3.3. The two cycles consist in four steps: adsorption (AD), blowdown (BD), purge (PG) and backfill (BF) and differ from each other only in the adsorption time (t_{ads}) and, subsequently, in the purge time (t_{pg}). The purge flow rate (Q_{purge}) was adapted for keeping the same *P/F*, according to Equation 3.2.

$$Q_{\text{purge}} = Q_{\text{feed}} P/F \frac{t_{\text{ads}}}{t_{\text{pg}}} \tag{3.2}$$

Table 3.3. Cyclic steps used in the two-column preliminary PSA tests: cycle 1.

Time (s)	2	t_{pg}	60	2	t_{pg}	60
Column 1	AD	AD	AD	BD	PG	BF
Column 2	BD	PG	BF	AD	AD	AD

Three-column tests were then performed, allowing the addition of an equalization step (PPE/DPE) without disrupting continuous production, according to the cycle described in Table 3.4. Further, an evacuation step was added to the cycle, enabling the unit to operate in VPSA mode (Table 3.5).

Table 3.4. Cyclic steps used in the three-column preliminary PSA test with equalization: cycle 2.

Time	2	2	116	2	2	116	2	2	116
Column 1	AD	AD	AD	DPE	BD	PG	PPE	BF	BF
Column 2	PPE	BF	BF	AD	AD	AD	DPE	BD	PG
Column 3	DPE	BD	PG	PPE	BF	BF	AD	AD	AD

Three VPSA preliminary tests were performed: with purging (test 1.4), without purging (test 1.5), and with vacuum purging (PGV) (test 1.6). Table 3.5 shows the generic cycle of the three VPSA tests. For the cycle with purging, this step is represented by PG and for the cycle with vacuum purging this step is represented by PGV. When there is no purge, the evacuation step replaces the time corresponding to PG/PGV.

Table 3.5. Cyclic steps used in the three-column preliminary VPSA tests: cycle 3.

Time	2	2	58	58	2	2	58	58	2	2	58	58
Column 1	AD	AD	AD	AD	DPE	BD	EV	PG/PGV	PPE	BF	BF	BF
Column 2	PPE	BF	BF	BF	AD	AD	AD	AD	DPE	BD	EV	PG/PGV
Column 3	DPE	BD	EV	PG/PGV	PPE	BF	BF	BF	AD	AD	AD	AD

Table 3.6. Operating conditions of all the preliminary tests performed at 9 bar with a feed flow rate of 1.70 $L_N \cdot min^{-1}$ and P/F equal to 0.05.

	Conditions				
	Test	**Cycle**	t_{ads} **(s)**	t_{pg} **(s)**	Q_{purge} **($L_N \cdot min^{-1}$)**
PSA	**1.1**	1	120	58	0.18
	1.2	1	600	538	0.09
	1.3	2	120	116	0.09
VPSA	**1.4**	3	120	58	0.18
	1.5	3	120	0	0
	1.6	3	120	58	0.18

3.3.2 Optimization

After analysing and discussing the results obtained in the preliminary tests, decision was made to proceed to a design of experiments (DoE) with the vacuum purged VPSA configuration. A DoE relates how the process parameters influence the response variables. It employs a statistical methodology to analyse experimental data and predict process properties when subjected to different conditions, within the limits defined in the initial experimental phase[40].

The factors under study and the corresponding imposed limits were the following:

- Adsorption time: 100 s to 180 s
- *P/F* ratio: 0 to 0.10
- Feed flow rate: 1.50 $L_N \cdot min^{-1}$ to 2.00 $L_N \cdot min^{-1}$

The DoE was built using the statistic software JMP. All the tests were performed at 9 bar using the cycle described in Table 3.7, where the value of t_1 depends on the adsorption time and is calculated by Equation 3.3.

$$t_1 = \frac{t_{\text{ads}} - 4}{2} \tag{3.3}$$

Table 3.7. Cyclic steps used in the optimization VPSA tests.

Time	2	2	t_1	t_1	2	2	t_1	t_1	2	2	t_1	t_1
Column 1	AD	AD	AD	AD	DPE	BD	EV	PGV	PPE	BF	BF	BF
Column 2	PPE	BF	BF	BF	AD	AD	AD	AD	DPE	BD	EV	PGV
Column 3	DPE	BD	EV	PGV	PPE	BF	BF	BF	AD	AD	AD	AD

Table 3.8. Operating conditions of the optimization tests.

Test	t_{ads} (s)	t_{pg} (s)	Q_{feed} ($L_N \cdot min^{-1}$)	*P/F*	Q_{purge} ($L_N \cdot min^{-1}$)
2.1	120	58	1.70	0	0
2.2	120	58	1.70	0.05	0.18
2.3	120	58	1.70	0.05	0.18
2.4	180	88	2.00	0	0
2.5	100	48	2.00	0	0
2.6	100	48	1.50	0	0
2.7	100	48	1.50	0.10	0.31
2.8	100	48	2.00	0.10	0.42
2.9	180	88	2.00	0.10	0.41
2.10	180	88	1.50	0.10	0.31
2.11	180	88	1.50	0	0
2.12	180	88	1.70	0.05	0.17
2.13	100	48	1.70	0.05	0.18
2.14	120	58	1.70	0.10	0.35
2.15	120	58	1.50	0.05	0.16
2.16	120	58	2.00	0.05	0.21

The effects of the factors were investigated in two responses (output variables):

- Water concentration in the product stream;
- Hydrogen recovery.

The mathematical model that correlates the output variables with the input variables is expressed by a quadratic polynomial model, obtained by least square regression[41]:

$$y_n = \beta_0 + \sum_{i=1}^{k} \beta_i X_i + \sum_{i<j}^{k} \beta_{ij} X_i X_j + \sum_{j=1}^{k} \beta_{jj} X_j^2 \qquad n = 1, \dots, n_r \tag{3.4}$$

where *y* is the response of the output variable; *k* is the number of input variables (=3); n_r is the number of response variables (=2); β_0 is the offset term; β_i, β_{ij} and β_{jj} are the regression coefficients and X_i and X_j are coded variables for the i^{th} and j^{th} parameter, respectively, according to Equations 3.5, 3.6 and 3.7. $\sum_{i=1}^{k} \beta_i X_i$ represents the linear influence of an individual parameter; $\sum_{i<j}^{k} \beta_{ij} X_i X_j$ corresponds to the effect of the interactions between individual parameters and $\sum_{j=1}^{k} \beta_{jj} X_j^2$ represents the non-linear behaviour of each parameter.

$$X_1 = \frac{P/F - \overline{P/F}}{\left(\frac{P/F_{+1} - P/F_{-1}}{2}\right)} \tag{3.5}$$

$$X_2 = \frac{t_{\text{ads}} - \overline{t_{\text{ads}}}}{\left(\frac{t_{\text{ads}_{+1}} - t_{\text{ads}_{-1}}}{2}\right)} \tag{3.6}$$

$$X_3 = \frac{Q_{\text{feed}} - \overline{Q_{\text{feed}}}}{\left(\frac{Q_{\text{feed}_{+1}} - Q_{\text{feed}_{-1}}}{2}\right)} \tag{3.7}$$

$\overline{P/F}$, $\overline{t_{\text{ads}}}$ and $\overline{Q_{\text{feed}}}$ represent the central points within the imposed limits of each coded variable. The +1 or -1 indexes represent the upper and lower limits, respectively.

Analysis of variance (ANOVA) was performed to evaluate the fit of the model. This analysis is performed using some statistical parameters, such as:

- p-value: ranges from 0 to 1 and gives the probability of the results were due to chance and not based on the model. The lower the p-value, more likely it is that a variance occurred because of the model.
- F-value: gives the ratio of explained variance to unexplained variance and represents the significance value for the test.
- Determination coefficient (R^2): represents the fraction of the variance of a dependent variable that can be explained by independent variables in a regression model.

The models obtained allow drawing the contour plots that are then used to evaluate the monitored responses within the entire experimental domain. It is then possible to map the optimal operating region of the VPSA process[42].

The process optimization was done by choosing the value of 5 ppm to match the target of water concentration desired and, simultaneously, maximizing the process recovery. Afterwards, the optimum set of parameters given by the software was tested using the same setup of Figure 3.3 and the cycle shown in Table 3.7.

3.3.3 VPSA test with a double-layered adsorbent bed

A test was also carried out with a double layer of adsorbent. The double layer consisted of about 23 g of alumina in the bottom layer and 7.5 g of zeolite 13X in the top layer.

According to the literature, zeolites have a higher water adsorption capacity, compared to alumina, when water is in lower concentrations. The test was performed under the same conditions as test 1.5 since this was the one where the highest value of product recovery was obtained.

3.4 Breakthrough curves

To have a better perception of the adsorbent behaviour concerning water vapor adsorption, a breakthrough experiment was performed.

The setup used was the one schematised in Figure 3.4. The dashed line that limits part of the installation represents a thermostatic chamber that allows the experiments to be performed in an isothermal environment. The temperature inside the chamber is measured by a thermocouple (TT) connected to a temperature controller (TC), which then sends a signal to a heater inside the chamber. The temperature set point defined in the controller was 30 ºC. The hydrogen that is fed in is controlled by an MFC and then enters the thermostatic chamber. Two manual three-way valves make it possible for the hydrogen to pass through the humidifier or to bypass it. Upstream, two more manual three-way valves also allow the feed stream to be fed into the base of the column or bypassed, going directly to the off gas. A manometer is placed in the off-gas line to read the pressure in the line and a PC to control it. At the end of the line, the dew point meter is placed to measure the humidity of the outlet stream from the installation. The two controllers are connected to a Bronkhorst control box, where it is possible to set and control the inlet flow rate and the pressure of the installation. The specifications of the MFC and PC used are detailed in Appendix B. The dew point meter and the humidifier were the same used for the PSA and VPSA tests.

The column was first pressurized with pure hydrogen and experiment begins when humid hydrogen enters the column. The water concentration is measured in the stream that exits the column and the experiment ends as soon as the water concentration at the outlet equals the one at the inlet. The experiment was carried out at 9 bar and with the optimum flow rate obtained in the optimization phase.

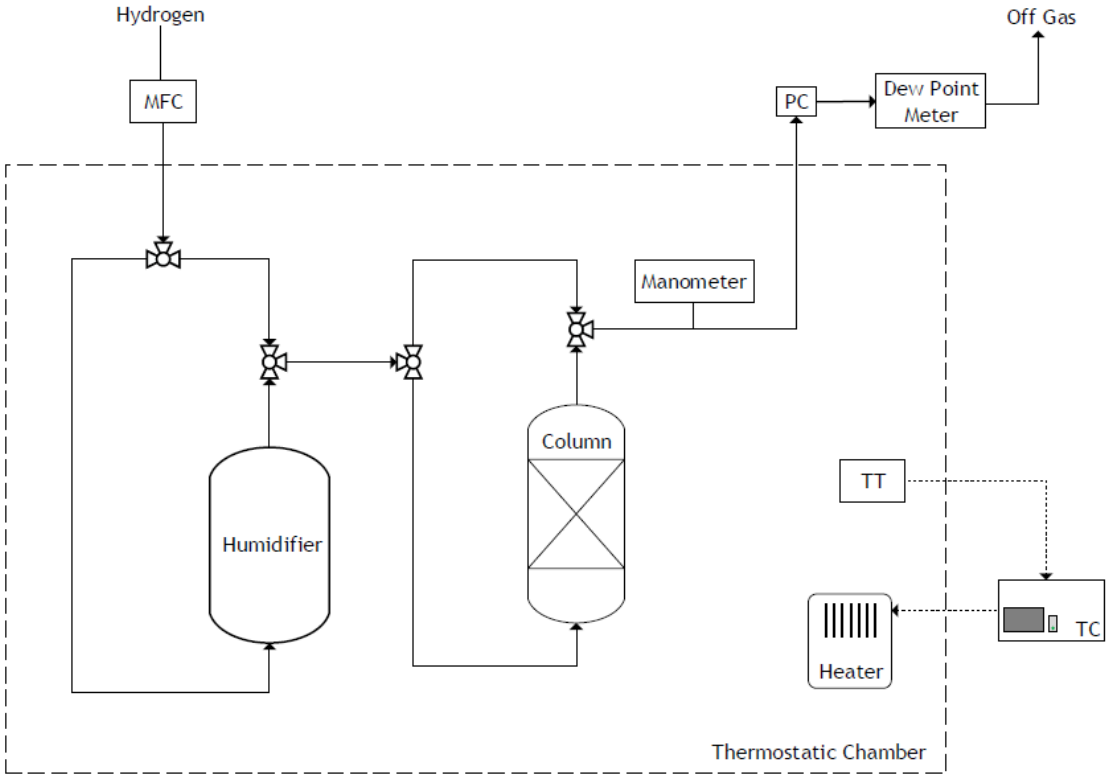

Figure 3.4. Setup used for the breakthrough experiments.

A breakthrough curve provides two crucial parameters used to evaluate the adsorption capacity of a packed column: the breakthrough time (t_{bp}) and the stoichiometric time (t_{st}), represented in Figure 3.5, that shows a typical breakthrough curve of a fixed-bed adsorption process. Breakthrough time was defined as the time at which the concentration of water at the outlet equals 5 ppm. If the breakthrough curve was an ideal stoichiometric front (vertical step in Figure 3.5), the total amount of water adsorbed was equal to the amount of water retained at stoichiometric time:

$$Q C_0 t_{st} = Q \int_0^{\infty} (C_0 - C)\, dt \tag{3.8}$$

Through the area above the breakthrough curve, the stoichiometric time can then be calculated:

$$t_{st} = \int_0^{\infty} \left(1 - \frac{C}{C_0}\right) dt \tag{3.9}$$

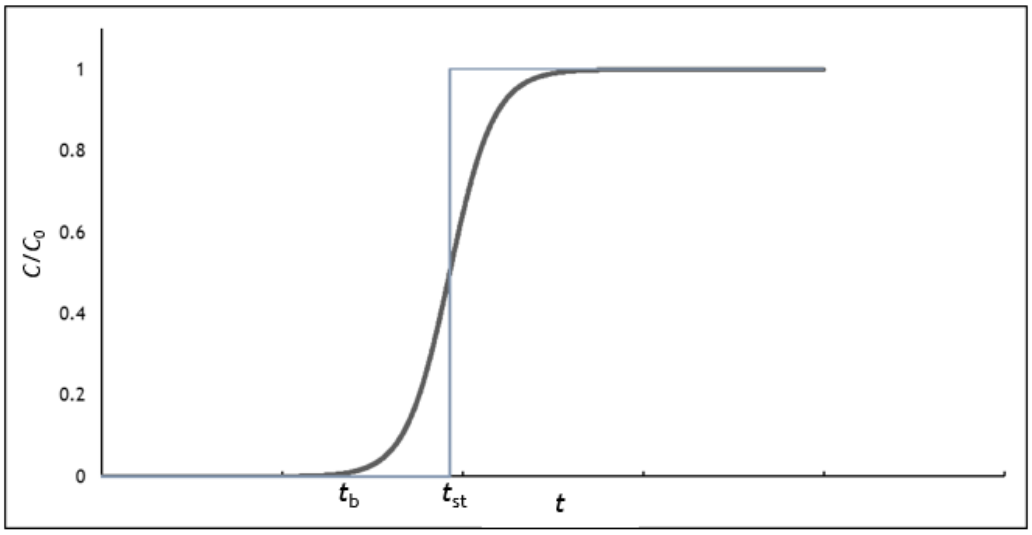

Figure 3.5. Typical breakthrough curve of a fixed-bed adsorption process.

Having these two parameters, one can then calculate the column efficiency (η) (Equation 3.10). The column efficiency is given by the ratio between the column capacity until the breakpoint (q_{bp}) (Equation 3.11) and the column total capacity (q_{tot}) (Equation 3.12). That is because the column should only operate until the breakpoint (5 ppm); after this, the gas outlet stream is contaminated and, therefore, the column should be regenerated.

$$\eta = \frac{q_{\mathrm{bp}}}{q_{\mathrm{tot}}} \tag{3.10}$$

$$q_{\mathrm{bp}} = \frac{C_0 Q \int_0^{t_{\mathrm{bp}}} \left(1 - \frac{C}{C_0}\right) \mathrm{d}t}{m_{\mathrm{ads}}} \tag{3.11}$$

$$q_{\mathrm{tot}} = \frac{C_0 Q \int_0^{\infty} \left(1 - \frac{C}{C_0}\right) \mathrm{d}t}{m_{\mathrm{ads}}} \tag{3.12}$$

Another parameter that can be obtained from the breakthrough curve and that also evaluates the capacity of the column for adsorption is the length of the mass transfer zone (L_{MTZ}). The mass transfer zone is defined as the zone in the adsorbent where mass transfer is still occurring between the gas phase and the adsorbent. Downstream of this zone, the water concentration in the adsorbent is in equilibrium with the concentration being fed, i.e., the adsorbent is saturated and upstream, the adsorbent has not yet been used[33]. In Figure 3.6, a diagram is represented where it is possible to observe the evolution of this zone along the column in several time intervals.

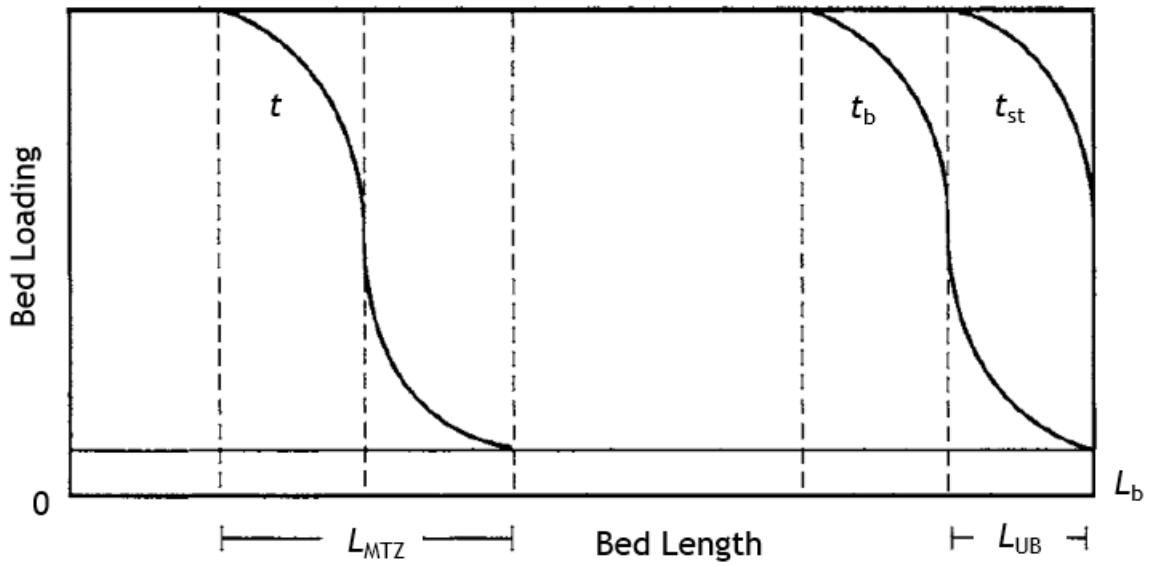

Figure 3.6. Mass transfer zone evolution along the bed. Adapted from (Kohl, et al., 1997)[33].

Observing Figure 3.6, one can see that the length of the MTZ (L_{MTZ}) is two times the length of unused bed (L_{UB}). The length of unused bed can be calculated, as given by (Rousseau, 1987)[43], through Equation 3.13:

$$LUB = \left(1 - \frac{t_{bp}}{t_{st}}\right) L_b = \frac{1}{2} L_{MTZ} \tag{3.13}$$

4 Results and Discussion

This section presents the results of all the PSA and VPSA tests performed, namely the preliminary tests and the optimization. The results were analysed in terms of hydrogen recovery and water content, namely considering a maximum allowable water concentration of 5 ppm, as required by the ISO 14687:2019; and a targeted recovery not lower than 90 %. The model obtained for optimizing the process is also presented as well as its statistical analysis. The experimental adsorption breakthrough curve corresponding to the optimum is presented at the end of the chapter.

4.1 Humidifier tests

Humidity tests were performed to verify the suitability of the humidifier to humidify a dry hydrogen stream, from the laboratory gas grid, up to the saturation point. The purpose was mimicking the electrolyser outlet. The tests showed that the humidifier was able to saturate hydrogen up to 93.6 %. Although full saturation was not reached, a feed slightly below the saturation point is typically preferred in a real process to avoid water condensation at the PSA outlet, which can damage the adsorbent materials irreversibly.

4.2 PSA and VPSA tests

4.2.1 Preliminary Tests

Six preliminary tests were performed to find the best performing setup configuration. The operating conditions of each of these tests and the corresponding experimental results are listed in Table 4.1.

In tests 1.1 and 1.2 only two columns were used, and the cycle time was varied, obtaining, in both, results far from the established goal. It can be observed that an increase in the cycle time (120 s to 600 s) leads to a decrease in the hydrogen purity (i.e. higher water concentration), while the opposite effect is observed for the recovery. This is explained by the fact that increasing the cycle time, the MTZ approaches the end of the column, increasing the concentration of water at the column outlet. On the other hand, recovery increases as result of less depressurizations in the same period, and therefore fewer losses.

In test 1.3, a third column was added, allowing the introduction of an equalization step in the cycle, while keeping continuous operation. As expected, the recovery increased, due to the lower pressure difference in the depressurisation stage and therefore reducing the blowdown losses. Despite the introduction of pressure equalization typically leads to a higher product contamination (considering the same pressure and cycle time), no significant changes were

observed in this case, 365 ppm in test 1.1 vs. 360 ppm in test 1.3. Although the purge quantity was the same, this discrepancy may be due to the different purge flow rate (0.18 $L_N \cdot min^{-1}$ during 58 s in test 1.1 vs. 0.09 $L_N \cdot min^{-1}$ during 116 s).

Table 4.1. Conditions and results of all the preliminary tests carried out at 9 bar with a feed flow rate of 1.70 $L_N \cdot min^{-1}$.

	Conditions					Results			
	Test	**Cycle**	t_{ads} **(s)**	t_{pg} **(s)**	Q_{purge} **($L_N \cdot min^{-1}$)**	R_H	**Water Concentration (ppm)**	**Dew Point ($°C_{atm}$)**	R_{rec}
PSA	**1.1**	1	120	58	0.18	1.30 %	365	-30.4	82.5 %
	1.2	1	600	538	0.09	2.09 %	588	-25.7	89.8 %
	1.3	2	120	116	0.09	1.28 %	360	-30.5	89.0 %
VPSA	**1.4**	3	120	58	0.18	0.42 %	118	-40.7	86.4 %
	1.5	3	120	0	0	0.55 %	155	-38.3	91.6 %
	1.6	3	120	58	0.18	0.08 %	26.5	-56.6	85.9 %

The results of the VPSA tests (runs 1.4, 1.5 and 1.6) revealed that the addition of the vacuum step resulted in a significant improvement in the purity of the output stream, a predictable outcome since vacuum regenerates the column more effectively which improves the working capacity of the adsorbent.

Comparing tests 1.4 (vacuum and purging at atmospheric pressure) and 1.5 (vacuum without purging), one can see that the elimination of the purge step leads to higher levels of impurity, although allowing achieving higher recovery (above 90 %). This results from the fact that the purging reduces the partial pressure of the adsorbed component, thus favouring desorption.

The purity levels can further be enhanced by purging simultaneously with vacuum, as shown by the results obtained in test 1.6. In terms of recovery, and comparing with test 1.4 (vacuum and purging at atmospheric pressure), no significant changes were observed. Accordingly, the configuration used in test 1.6 was chosen for process optimization by means of a design of experiments.

4.2.2 Optimization

According to the preliminary tests, cycle 3 is the most efficient in terms of purity and recovery. The cycle was optimized through a DoE using three factors: the adsorption time, t_{ads}, the purge to feed ratio, *P*/*F*, and the feed flow rate. The result was a DoE with 16 experiments, whose results are presented in Table 4.2.

Table 4.2. Operating conditions and results of the optimization tests.

Conditions						Results			
Test	t_{ads} **(s)**	t_{pg} **(s)**	Q_{feed} **($L_N \cdot min^{-1}$)**	***P/F***	Q_{purge} **($L_N \cdot min^{-1}$)**	R_H	**Water Concentration (ppm)**	**Dew Point (°C_{atm})**	R_{rec}
2.1	120	58	1.70	0	0	0.62 %	174	-38.3	91.6 %
2.2	120	58	1.70	0.05	0.18	0.08 %	22.5	-55.1	85.9 %
2.3	120	58	1.70	0.05	0.18	0.08 %	22.5	-55.1	85.9 %
2.4	180	88	2.00	0	0	0.80 %	242	-34.2	90.6 %
2.5	100	48	2.00	0	0	0.51 %	160	-43.0	88.5 %
2.6	100	48	1.50	0	0	0.12 %	44.7	-52.8	87.7 %
2.7	100	48	1.50	0.10	0.31	0.01 %	3.44	-67.9	76.9 %
2.8	100	48	2.00	0.10	0.42	0.01 %	4.03	-67.7	78.4 %
2.9	180	88	2.00	0.10	0.41	0.01 %	3.60	-67.8	83.6 %
2.10	180	88	1.50	0.10	0.31	0.01 %	4.00	-67.3	79.3 %
2.11	180	88	1.50	0	0	0.17 %	54.6	-50.9	86.3 %
2.12	180	88	1.70	0.05	0.17	0.07 %	23.9	-54.9	85.4 %
2.13	100	48	1.70	0.05	0.18	0.01 %	5.93	-65.6	80.3 %
2.14	120	58	1.70	0.10	0.35	0.01 %	4.00	-67.9	78.5 %
2.15	120	58	1.50	0.05	0.16	0.01 %	4.00	-67.7	81.4 %
2.16	120	58	2.00	0.05	0.21	0.01 %	4.01	-67.9	84.6 %

Experimental results demonstrate that the performance of a PSA unit is a trade-off between product purity and recovery, i.e., a higher purity usually means a lower recovery and vice versa. Similar conclusions are typically taken by other researchers in PSA studies[44,45].

With the results attained, by least squares regression, second order polynomial models for the two responses were obtained in the JMP software. These models allowed to describe the process responses, water concentration and hydrogen recovery, as function of the process parameters *P/F* ratio, feed flow rate and adsorption time. The obtained parameters (β_0, β_{ij}, β_{jj}) of the second order polynomial empiric models (Equation 3.4) are given in Table 4.3, for the two responses: water concentration ($n = 1$) and product recovery ($n = 2$).

Table 4.3. Parameters of the response models. n=1 for water content and n=2 for recovery.

	n	
	1	**2**
β_0	38.2	0.86
β_1	-67.9	-0.05
β_2	11.4	0.007
β_3	31.5	0.01
β_{12}	-7.84	0.01
β_{13}	-36.4	0.01
β_{23}	12.0	-0.01
β_{11}	66.8	0.01
β_{22}	-16.0	0.001
β_{33}	-24.5	-0.02

Table 4.4 shows the models predictions to both responses compared to the results obtained experimentally, for each optimization test.

Table 4.4. Predicted outcomes from the model compared with the experimental results.

Conditions				**Experimental Results**		**Predicted Results**	
Test	t_{ads} **(s)**	Q_{feed} **($L_N \cdot min^{-1}$)**	***P/F***	**Water Concentration (ppm)**	R_{rec}	**Water Concentration (ppm)**	R_{rec}
2.1	120	1.70	0	174	91.6 %	146	91.0 %
2.2	120	1.70	0.05	22.5	85.9 %	22.4	84.6 %
2.3	120	1.70	0.05	22.5	85.9 %	22.4	84.6 %
2.4	180	2.00	0	242	90.6 %	231	90.7 %
2.5	100	2.00	0	160	88.5 %	169	88.7 %
2.6	100	1.50	0	44.7	87.7 %	57.3	87.4 %
2.7	100	1.50	0.10	3.44	76.9 %	9.96	75.7 %
2.8	100	2.00	0.10	4.03	78.4 %	0	77.6 %
2.9	180	2.00	0.10	3.60	83.5 %	7.34	83.7 %
2.10	180	1.50	0.10	4.00	79.3 %	0	79.2 %

Conditions				Experimental Results		Predicted Results	
Test	t_{ads} **(s)**	Q_{feed} **($L_N \cdot min^{-1}$)**	***P/F***	**Water Concentration (ppm)**	R_{rec}	**Water Concentration (ppm)**	R_{rec}
2.11	180	1.50	0	54.6	86.3 %	71.8	86.8 %
2.12	180	1.70	0.05	23.9	85.4 %	24.0	84.7 %
2.13	100	1.70	0.05	5.93	80.3 %	5.93	82.3 %
2.14	120	1.70	0.10	4.00	78.5 %	32.5	80.5 %
2.15	120	1.50	0.05	4.00	81.4 %	0	82.6 %
2.16	120	2.00	0.05	4.01	84.6 %	29.5	84.8 %

Figure 4.1 depicts the standardized effects (t-ratio) of each response, i.e., the estimates (β parameters) divided the respective standard deviations. The vertical red line is a reference value for statistically significant values, at a 95 % confidence level. Above the modulus of this value, one can consider that the parameter has a significant effect in the model. The values represented in the chart are listed in Appendix C.

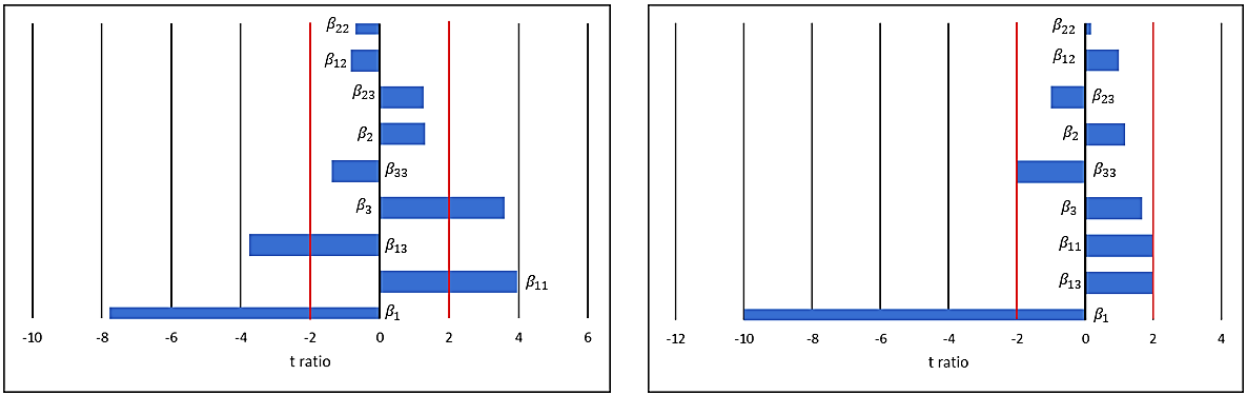

Figure 4.1. Standardized effects of the water concentration model (at the left) and recovery model (at the right).

Accordingly, it can be concluded that, under the studied conditions, the *P/F* ratio is the parameter with major influence in both water content and hydrogen recovery, whose effect is mainly linear (β_1), although the quadratic effect, given by β_{11} , is also significant in the case of the water content. In addition, the feed flow rate and its combined effect with the *P/F* are also statistically significant for the water content, β_3 and β_{13}, respectively. In turn, for the product recovery, only the linear effect of the *P/F* ratio is statistically significant.

In practice, this means that an increase in the *P/F* results in a produced hydrogen with lower water content (higher purity), but with a lower recovery rate. This occurs because a higher

purge quantity regenerates the column more effectively, thus leading to a better efficiency of the subsequent adsorption step. However, since the purge is carried out with part of the produced hydrogen, the greater the purge, the greater is the loss of hydrogen to off gas (waste gas).

On the other hand, an increase in the feed flow rate results in an increased hydrogen contamination, i.e. higher water concentration. This happens because, for the same time period, a greater amount of gas is available to adsorb. Thus, the adsorbent saturates faster, consequently increasing the concentration of the heavy component (water) in the product stream. On the other hand, while the feed rate increases, the production rate also increases consequently, and therefore there is no great influence of this parameter on the recovery.

At last, it is noticeable by analysing the charts in Figure 4.1, that the cycle time does not play a very significant role in the PSA responses, when within the imposed limits (100-180 s). However, as already mentioned and analysed before, the cycle time can have a decisive effect on the equipment efficiency. In this case, the adsorption time is sufficiently large so that the blowdown losses, i.e. waste gas released during depressurization, are very small when compared to produced hydrogen.

It is important to note that the conclusions drawn from the statistical model are only applicable within the limits of the independent variables domain. It is not possible to extrapolate the same conclusions outside the established boundaries.

ANOVA was also performed to assess the adaptability and significance of the model to the experimental data. p-value, F-value and R^2 for each response model are displayed in Table 4.5.

Table 4.5. ANOVA parameters obtained for each model.

Model	F-ratio	p-value	R^2
Water concentration	11.7	0.0037	0.95
Recovery	12.2	0.0032	0.95

The obtained p-values are low enough to conclude that the model is significant with respect to the experimental data. Likewise, the r-squared value allows for the conclusion that 95 % of the variation in the dependent factors can be explained by the independent variables of the quadratic model. It can then be considered that the model is able to explain the responses of the process successfully and can be used within the limits already mentioned for the initial parameters.

The prediction profiler, i.e., the predicted values for water concentration and recovery in function of *P*/*F* ratio, feed flow rate and adsorption time are plotted in Figure 4.2.

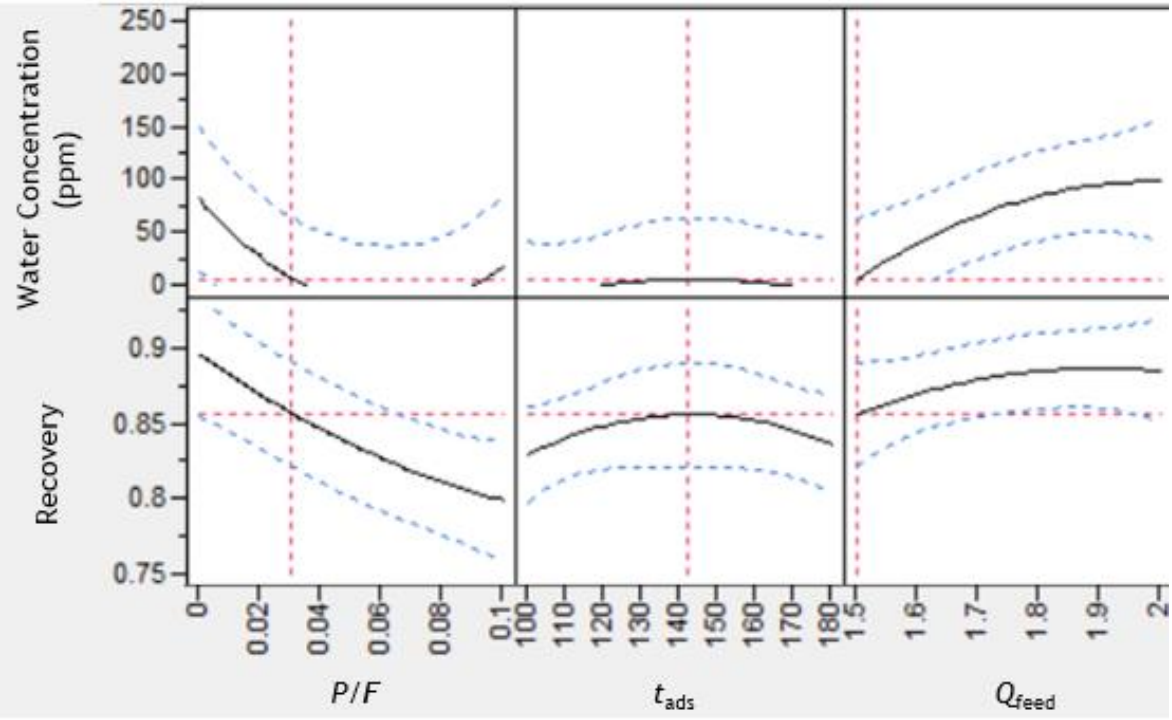

Figure 4.2. Predicted results as a function of P/F ratio, adsorption time and feed flow rate. Extracted from the JMP software.

Using the obtained fitting models, the operating conditions were optimized using the desirability function of JMP software for coding the optimal conditions. In this case, water concentration was set to match 5 ppm and recovery was set to be maximized. The parameters given by the software to achieve this goal are in Table 4.6, as well as the results predicted by the models.

Table 4.6. Optimum parameters and predicted results.

Conditions			**Predicted Results**	
t_{ads} (s)	**Q_{feed} ($L_N \cdot min^{-1}$)**	***P/F***	**Water Concentration (ppm)**	**Recovery**
142	1.50	0.03	5	85.6 %

When tested experimentally, the conditions presented allowed to obtain a recovery of 85.6 % with a water concentration in the product of 4.00 ppm. This result is close to the one predicted by the model and meets the targeted water concentration of less than 5 ppm, the limit value established by the ISO 14687:2019.

It should be noted that the dew point meter used has a detection limit of 3 ppm. Therefore, the experiments that resulted in water contents closer to this limit may be even lower. Using a dew point meter with a lower detection limit would overcome this situation and could result in a better optimization of the system.

Almost all the values obtained for the recovery are below 90 %, which was the initial target of this work. To achieve recoveries very close to 100 %, it is recommended to implement a recycle to the wet hydrogen leaving the PSA, at the purge, blowdown or vacuum steps. This configuration is schematized in Figure 4.3. Briefly, the wet hydrogen leaving the PSA is at 0 or 1 bar, therefore needing recompression so that it can be recycled to the PSA. As it is compressed, the temperature rises and a heat exchanger needs to be installed to lower the temperature of the mixture after the compressor. To remove excess water, a liquid gas separator is also installed after the heat exchanger. In this separator, there will always be some loss of hydrogen for purging.

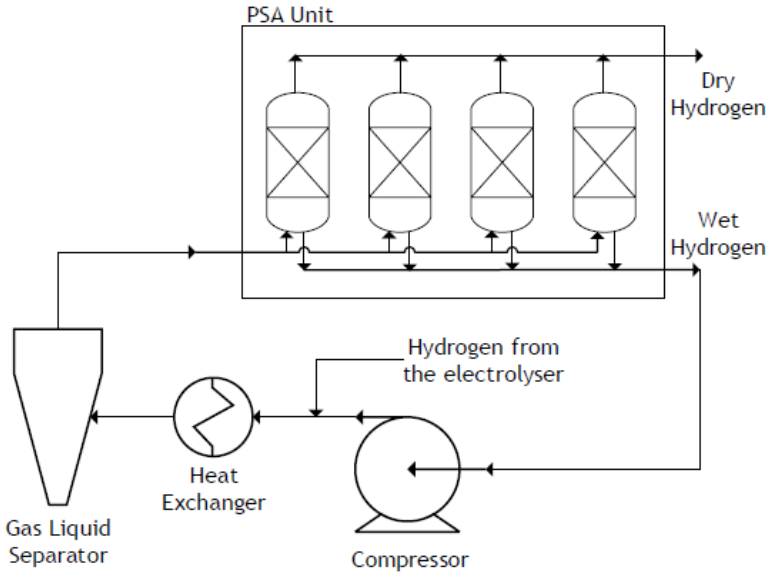

Figure 4.3. Possible setup of a high scale hydrogen drying unit with a recycle of the off-gas stream.

4.2.3 VPSA test with a double-layered adsorbent bed

Since literature often refers the use of multiple layers in gas drying for achieving lower dew points[37], the conditions used in test 1.5 were repeated, now using two adsorbent layers: activated alumina and zeolite 13X. This resulted in an output water concentration of 302 ppm with a recovery of 91.6 %. Compared with test 1.5, where a concentration of 174 ppm with the same recovery was obtained, one can observe that the purity of the outlet stream decreases with the addition of the zeolite layer. This result goes against the initially expected but can, however, be explained by the decrease in capacity of zeolite 13X, when at steady state. According to previous studies, the zeolite 13X loses 44.2 % of its capacity when at steady state. Activated alumina, on the other hand, only loses 21.1 %[27]. Moreover, the amount of zeolite that was placed in the columns may not correspond to the optimum quantity of this adsorbent. That is, since zeolite 13X presents a higher adsorption capacity at low water concentrations, the

water content that reached the zeolite layer could be still too high, thus compromising the regenerability of the material.

For future work, it is recommended to test different ratios of activated alumina and zeolite 13X, or other zeolites (e.g. zeolite 4A). Also alternative configurations, namely a triple layer of adsorbents could be also tested, specifically the bottom layer would be silica gel to protect the up-stream bed from water condensation; the intermediate layer would be of activated alumina which would adsorb most of the water; and the top layer would be zeolite 4A to remove trace concentrations of water. According to (Robson, 1961)[46], the best adsorbent for water adsorption in vacuum systems is zeolite 4A. In comparison with activated alumina and silica gel, at steady state, zeolite 4A showed sixteen times higher water adsorption capacity than silica and almost five times higher than alumina. The study of this configuration should, however, be accompanied by a study of the optimum quantities of each adsorbent in each layer.

4.3 Breakthrough Curves

To analyse the effluent composition (water vapor) vs. time during adsorption step, a breakthrough experiment was performed to assess the adsorption column dynamics behaviour. The experiment was performed at a pressure of 9 bar and using a flow rate of 1.50 $L_N \cdot min^{-1}$, the same conditions of the optimum. The obtained breakthrough curve is represented in Figure 4.4. The ideal stoichiometric front is represented by the vertical step blue line.

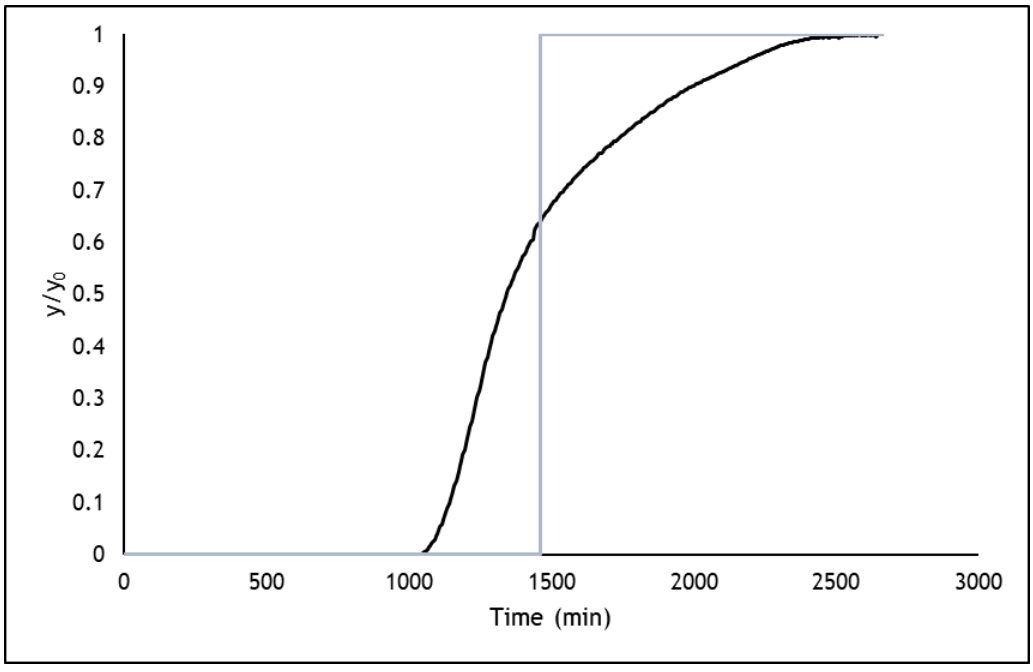

Figure 4.4. Effective breakthrough curve performed with 1.50 $L_N \cdot min^{-1}$ at 9 bar.

The stoichiometric time (t_{st}) was calculated using the area above the breakthrough curve. A value of about 1461 minutes was obtained. The breakthrough of the column, that is, the moment at which it begins to exit wet hydrogen was observed at about 1050 minutes after the beginning of the experiment. From this point on, the column is no longer able to produce dry hydrogen and the water concentration at the exit gradually increases.

With the stoichiometric and time and the breakthrough time, it was then possible to calculate the column efficiency, the length of unused bed and the length of the mass transfer zone, using Equations 3.10 and 3.13. The column has an efficiency of 55.1 %, a length of unused bed of 2.23 cm and the mass transfer zone has 4.46 cm. The MTZ then occupies 56.2 % of the column.

The columns are therefore able of purifying the hydrogen stream. Using longer columns could, however, improve these parameters. Usually, the MTZ occupies about 20 % of the column total length. The optimum column length for this type of adsorption would, then, be higher than 25 cm. The use of longer columns brings, however, the disadvantage of an increase in the time required to reach cyclic steady state. Each PSA test with the columns used in this work took about 24 hours to reach cyclic steady state. With larger columns, the stabilization time would be even longer. To have a trade-off between stabilization time and column length, it would be reasonable to use columns of about 17 cm, where the MTZ would occupy about 25 % of the column.

5 Conclusion

The main objective of this work was the optimization of a PSA setup for hydrogen drying to obtain a hydrogen stream with less than 5 ppm of water and with a maximum recovery. The goal was partially fulfilled since the minimum water content was achieved but at the expense of low recoveries.

The preliminary PSA and VPSA experiments allowed to choose the best process configuration to be optimized. The setup chosen was a three column, vacuum purged VPSA, since this was the one that had the best balance between product purity and recovery.

A Design of Experiments, using the Response Surface Methodology, allowed to obtain an empiric second order polynomial model that relates the operating conditions and the response variables: water concentration and recovery. Using this model it was possible to conclude that the purge to feed ratio was the main factor affecting the performance of the process, followed by the feed flow rate. On the other hand, the adsorption time displayed the least role of the variables characterising the performance of the process. It must be emphasised however, that these conclusions are only valid within the selected operating conditions domain. The second order polynomial model allowed to find the best operating conditions: the *P*/*F* ratio was 0.03, the feed flow rate was 1.50 $L_N \cdot min^{-1}$ and the adsorption time was 142 s. The experimental VPSA response to these parameters was 4.00 ppm for the water concentration and 85.6 % of recovery.

An adsorbent layered-VPSA approach was assessed, using a first layer of alumina, occupying 80 % of the column, and a second of zeolite 13X, occupying the remaining 20 %. The obtained separation performance was worse. However, the zeolite loading was not optimized, and this conclusion must be taken as preliminary. Further research should be conducted to optimise an adsorbent layered VPSA unit.

Performing a breakthrough experiment, allowed to conclude that the columns used in all the experiments were able of drying hydrogen with a 55.1 % efficiency. Longer columns should be used to increase this efficiency.

In conclusion, the goal of the optimization of the hydrogen drying unit was partially reached since the target for water concentration at the outlet was met but with a low recovery.

6 Assessment of the work done

6.1 Objectives Achieved

As mentioned in the *Introduction* chapter, the first objective of this work was to carry out preliminary tests to find the configuration that best fitted the defined objective. This goal was achieved, reaching the aforementioned three-column VPSA configuration.

The second objective was to optimize the process through a DoE. This objective was partially fulfilled since the water concentration target was reached but at the expense of a low recovery.

6.2 Other Work Carried Out

During this work, it was possible to perform some other PSA tests with other gas mixtures, such as carbon monoxide and carbon dioxide. It was also possible to assist and support the assembly of other large scale PSA units.

6.3 Final Assessment

The work developed in this dissertation was very rewarding. Besides the study developed, I was able to learn about automation, how to assemble a laboratory set-up and how to search for gas leaks. This work allowed me to develop my problem-solving skills and, most of all, allowed me to develop my personal skills.

Hydrogen drying through PSA is a developing field that still has a long way to go. Several other configurations and other types of adsorbents that were not thoroughly addressed in this dissertation can still be studied. So, for future studies, my suggestions are:

- Performing breakthrough experiments on larger columns.
- Studying the water adsorption capacity of silica gel.
- Finding the optimum quantity of zeolite 13X in a double-layered adsorbent bed with alumina.
- Testing a three-adsorbent bed with silica, alumina and zeolite 4A.
- Performing a four-column test.
- Check for a more sensitive dew point meter.
- Placing the entire installation in an isothermal environment to optimize the operation of the humidifier.

7 References

1. Züttel A, Remhof A, Borgschulte A, Friedrichs O. Hydrogen: the future energy carrier. *Philosophical Transactions of the Royal Society A: Mathematical, Physical and Engineering Sciences*. 2010;368(1923):3329-3342.
2. International Energy Agency. *The Future of Hydrogen: seizing today's opportunities*. 2019.
3. International Renewable Energy Agency. *Green hydrogen cost reduction*. 2020.
4. National Grid. The hydrogen colour spectrum. 2022; https://www.nationalgrid.com/stories/energy-explained/hydrogen-colour-spectrum. Accessed 27/04/2022.
5. CIC EnergiGUNE. The electrolisys of water: a sustainable way to produce green hydrogen. 2022; https://cicenergigune.com/en/blog/electrolysis-water-sustainable-produce-green-hydrogen. Accessed 09/05/2022.
6. Ligen Y, Vrubel H, Girault H. Energy efficient hydrogen drying and purification for fuel cell vehicles. *International Journal of Hydrogen Energy*. 2020;45(18):10639-10647.
7. International Organization for Standardization. Hydrogen fuel quality — Product specification. 2019.
8. Sundén B. Chapter 3 - Hydrogen. In: Sundén B, ed. *Hydrogen, Batteries and Fuel Cells*: Academic Press; 2019:37-55.
9. Nicita A, Maggio G, Andaloro APF, Squadrito G. Green hydrogen as feedstock: Financial analysis of a photovoltaic-powered electrolysis plant. *International Journal of Hydrogen Energy*. 2020;45(20):11395-11408.
10. The Royal Society. #2050challenge – Reaching net zero emissions by 2050. https://royalsociety.org/whats-new/2050-challenge/. Accessed 30/05/2022.
11. International Energy Agency. *Global Hydrogen Review 2021*. 2021.
12. Millet P, Grigoriev S. Chapter 2 - Water Electrolysis Technologies. In: Gandía LM, Arzamendi G, Diéguez PM, eds. *Renewable Hydrogen Technologies*. Amsterdam: Elsevier; 2013:19-41.
13. Bouckaert S, Pales AF, McGlade C, et al. Net Zero by 2050: A Roadmap for the Global Energy Sector. 2021.
14. Mead NV. Fuel of the future: How to realize the potential of hydrogen. 2022; https://www.weforum.org/agenda/2022/03/hydrogen-decarbonization-climate-change-energy. Accessed 07/06/2022.
15. European Comission. A hydrogen strategy for a climate-neutral Europe. 2020.
16. Kayfeci M, Keçebaş A, Bayat M. Chapter 3 - Hydrogen production. In: Calise F, D'Accadia MD, Santarelli M, Lanzini A, Ferrero D, eds. *Solar Hydrogen Production*: Academic Press; 2019:45-83.
17. Enapter. AEM Water Electrolysis: How it Works. 2020; https://www.enapter.com/newsroom/aem-water-electrolysis-how-it-works. Accessed 07/06/2022.
18. Brinner A, Philipps F. Hydrogen as the Fuel of the Future-Production; Purification; Storage. *Tagungsband Motor & Umwelt 2001*. 2001.
19. McCay MH, Shafiee S. 22 - Hydrogen: An Energy Carrier. In: Letcher TM, ed. *Future Energy (Third Edition)*: Elsevier; 2020:475-493.

20. Miller HA, Bouzek K, Hnat J, et al. Green hydrogen from anion exchange membrane water electrolysis: a review of recent developments in critical materials and operating conditions. *Sustainable Energy & Fuels*. 2020;4(5):2114-2133.

21. Carmo M, Fritz DL, Mergel J, Stolten D. A comprehensive review on PEM water electrolysis. *International Journal of Hydrogen Energy*. 2013;38(12):4901-4934.

22. Hussy C. Water electrolysis explained – the basis for most Power-to-X processes. 2022; https://ptx-hub.org/water-electrolysis-explained/. Accessed 30/06/2022.

23. Smolinka T. FUELS – HYDROGEN PRODUCTION | Water Electrolysis. In: Garche J, ed. *Encyclopedia of Electrochemical Power Sources*. Amsterdam: Elsevier; 2009:394-413.

24. Chen P, Hu X. High-Efficiency Anion Exchange Membrane Water Electrolysis Employing Non-Noble Metal Catalysts. *Advanced Energy Materials*. 2020;10(39):2002285.

25. Commonwealth Scientific and Industrial Research Organisation. Anion exchange membrane (AEM) electrolysis. 2022; https://www.csiro.au/en/work-with-us/ip-commercialisation/hydrogen-technology-marketplace/anion-exchange-membrane-aem-electrolysis. Accessed 08/06/2022.

26. Ruthven DMFSKKS. *Pressure swing adsorption*. [New York]; [Weinheim]; [Cambridge]: VCH; 1994.

27. Bexiga R. *Development of a Hydrogen Drying Unit by Adsorption Processes* [Master Thesis], Faculty of Engineering of the University of Porto; 2021.

28. Cruz P. *Simulação e Optimização de Processos Cíclicos de Adsorção*, Ph. D. Thesis, Universidade do Porto, Porto, Portugal; 2003.

29. Liow J-L, Kenney CN. The backfill cycle of the pressure swing adsorption process. *AIChE Journal*. 1990;36(1):53-65.

30. Mike Peters KH, Huyen Dinh. *Renewable Electrolysis Integrated Systems Development and Testing*. 2015.

31. Mike Peters KH, Huyen Dinh. *Renewable Electrolysis Integrated Systems Development and Testing*. 2016.

32. Yorick Ligen HG, Jakob Rager. *Combined service station for battery electric & hydrogen fuel cell vehicles*. Swiss Federal Office of Energy;2018.

33. Kohl AL, Nielsen RB. Chapter 12 - Gas Dehydration and Purification by Adsorption. In: Kohl AL, Nielsen RB, eds. *Gas Purification (Fifth Edition)*. Houston: Gulf Professional Publishing; 1997:1022-1135.

34. BASF. Adsorbents Solutions for Compressed Air Drying. 2021; https://catalysts.basf.com/files/literature-library/BASF_CAT-002485_Sorbead_Air_Broschuere_Update_03.pdf,. Accessed 25/06/2022.

35. Activated Alumina Balls. Dew Point that Activated Alumina can reach. 2020; https://www.activatedaluminaballs.com/blogs/dew-point-that-activated-alumina-can-reach. Accessed 08/04/2022.

36. Ferreira D, Magalhães R, Taveira P, Mendes A. Effective Adsorption Equilibrium Isotherms and Breakthroughs of Water Vapor and Carbon Dioxide on Different Adsorbents. *Industrial & Engineering Chemistry Research*. 2011;50(17):10201-10210.

37. Rege SU, Yang RT, Qian K, Buzanowski MA. Air-prepurification by pressure swing adsorption using single/layered beds. *Chemical Engineering Science*. 2001;56(8):2745-2759.

38. Grace WR. Product Information SYLOBEAD AA 102. 2017.

39. BASF. Product Data Sheet - BASF 13X Molecular Sieve. 2020.

40. Wagner JR, Mount EM, Giles HF. 25 - Design of Experiments. In: Wagner JR, Mount EM, Giles HF, eds. *Extrusion (Second Edition)*. Oxford: William Andrew Publishing; 2014:291-308.

41. Kusworo T, Songip A, Amin N. Optimization of Partial Oxidation of Methane for Hydrogen Production on NiO-CoO/MgO Catalyst using Design of Experiment. *IJET-IJENS*. 2010;10(1):1-8.

42. Quirino PPS, Amaral A, Manenti F, Pontes KV. Mapping and optimization of an industrial steam methane reformer by the design of experiments (Doe). *Chemical Engineering Research and Design*. 2022.

43. Rousseau RW. *Handbook of separation process technology*. John Wiley & Sons; 1987.

44. Luberti M, Friedrich D, Brandani S, Ahn H. Design of a H2 PSA for cogeneration of ultrapure hydrogen and power at an advanced integrated gasification combined cycle with pre-combustion capture. *Adsorption*. 2014;20(2):511-524.

45. Relvas F, Whitley RD, Silva C, Mendes A. Single-Stage Pressure Swing Adsorption for Producing Fuel Cell Grade Hydrogen. *Industrial & Engineering Chemistry Research*. 2018;57(14):5106-5118.

46. Robson EM. The vacuum use of molecular sieves and other desiccants. *Vacuum*. 1961;11(1):10-15.

Annex A Hydrogen Fuel Quality - Product Specification

Deployment of hydrogen fuel cells for stationery and transportation applications calls for the development of quality standards for hydrogen. ISO 14687:2019 specifies the minimum quality characteristics for hydrogen fuel used in stationary and vehicular applications as listed in Table A.1. Hydrogen is classified by type, grade and category as follows[7]:

- Type I, Grade D: gaseous hydrogen for PEM fuel cell road vehicle systems.
- Type II, Grade D: liquid hydrogen fuel for PEM fuel cell road vehicle systems.
- Type I, Grade E, Category I: gaseous hydrogen fuel for PEM fuel cell applications for stationary systems (high efficiency applications: 50 % minimum hydrogen).
- Type I, Grade E, Category 2: gaseous hydrogen fuel for PEM fuel cell applications for stationary systems (high load applications: 50 % minimum hydrogen).
- Type I, Grade E, Category 3: gaseous hydrogen fuel for PEM fuel cell applications for stationary systems (high fuel index hydrogen applications: 99.9 % minimum hydrogen).

Table A 1. Maximum impurity concentration allowed for hydrogen fuel in stationery and road applications. Adapted from (International Organization for Standardization, 2019)[7].

Component	**Maximum impurity concentration (in µmol·mol^{-1} unless stated)**			
	Types I and II, Grade D	**Type I, Grade E, Cat. 1**	**Type I, Grade E, Cat. 2**	**Type I, Grade E, Cat. 3**
Water	5	Non-condensing at ambient conditions	Non-condensing at ambient conditions	Non-condensing at ambient conditions
Total hydrocarbons compounds as methane basis	2	10	2	2
Oxygen	5	200	200	5
Helium	300	400000	400000	1000
Nitrogen	100	400000	400000	1000
Argon	100	400000	400000	1000
Carbon dioxide	2	Included in total non-hydrogen gases' (max. 50 % mol·mol^{-1})	Included in total non-hydrogen gases' (max. 50 % mol·mol^{-1})	2
Carbon monoxide	0.2	10	10	0.2

Component	Maximum impurity concentration (in µmol·mol^{-1} unless stated)			
	Types I and II, Grade D	Type I, Grade E, Cat. 1	Type I, Grade E, Cat. 2	Type I, Grade E, Cat. 3
Total sulphur compounds	0.004	0.004	0.004	0.004
Formaldehyde	0.01	3	0.01	0.01
Formic acid	0.2	12	0.2	0.2
Ammonia	0.1	0.1	0.1	0.1
Total halogenated compounds	0.05	0.05	0.05	0.05
Particulate concentration	1 mg·kg^{-1}	1 mg·kg^{-1}	1 mg·kg^{-1}	1 mg·kg^{-1}

Appendix A Specifications of the equipment used in the PSA and VPSA tests

Hydrogen Flow Controller

- Brand: Bronkhorst
- Maximum Flow Rate: 10 $L_N \cdot min^{-1}$ N_2
- Control Valve: Normally Closed

Nitrogen Flow Controller

- Brand: Bronkhorst
- Maximum Flow Rate: 2 $L_N \cdot min^{-1}$ N_2
- Control Valve: Normally Closed

Purge Flow Controller

- Brand: Bronkhorst
- Maximum Flow Rate: 1 $L_N \cdot min^{-1}$ Air
- Control Valve: Normally Closed

Backfill and Product Flow Meters

- Brand: Bronkhorst
- Maximum Flow Rate: 3 $L_N \cdot min^{-1}$ Air

Pressure Controller

- Brand: Bronkhorst
- Pressure Range: 0/10 bar
- Maximum Flow Rate: 5 $L_N \cdot min^{-1}$ N_2

Dew Point Meter

- Brand: Vaisala
- Model: DMP74B
- Dew Point range measured at 1 atm: -80 ºC to +20 ºC
- Accuracy: ± 2 ºC

Vacuum Pump

- Brand: Vacuubrand
- Vacuum pressure: $4 \cdot 10^{-4}$ mbar
- Maximum Flow Rate: 2.3/2.8 $m^3 \cdot h^{-1}$
- Power: 0.18 kW

Appendix B Specifications of the equipment used in the breakthrough experiment

Hydrogen Flow Controller

- Brand: Bronkhorst
- Maximum Flow Rate: 2 $L_N \cdot min^{-1}$ Air
- Control Valve: Normally Closed

Pressure Controller

- Brand: Bronkhorst
- Pressure Range: 1/10 bar
- Maximum Flow Rate: 5 $L_N \cdot min^{-1}$ N_2

Temperature Controller

- Brand: Eurotherm
- Model: 2216L
- Temperature Range: 0-55 ºC

Appendix C Sorted Parameter Estimates

Water Concentration

Table A 2. Sorted parameter estimates for the water concentration model.

Term	Estimate	Standard Error	t Ratio
β_{22}	-16.0	23.2	-0.69
β_{12}	-7.84	9.46	-0.83
β_{23}	12.0	9.42	1.28
β_{2}	11.4	8.67	1.32
β_{33}	-24.5	17.7	-1.38
β_{3}	31.5	8.72	3.61
β_{13}	-36.4	9.65	-3.77
β_{11}	66.8	16.9	3.95
β_{1}	-67.9	8.72	-7.78

Product Recovery

Table A 3. Sorted parameter estimates for the product recovery model.

Term	Estimate	Standard Error	t Ratio
β_{22}	0.001	0.006	0.26
β_{12}	0.01	0.01	1.12
β_{23}	-0.01	0.01	-1.17
β_{2}	0.01	0.006	1.20
β_{33}	-0.02	0.010	-1.70
β_{3}	0.01	0.006	1.67
β_{13}	0.01	0.005	2.00
β_{11}	0.01	0.005	2.00
β_{1}	-0.05	0.005	-9.11